



Polyether Ketone Ketone (PEKK) matrix composites for material extrusion additive manufacturing

Kaifur Rashed^{1,2} · Abdullah Kaf¹ · Ranya Simons² · Mel Dell'Olio² · Stuart Bateman¹

Received: 22 September 2023 / Accepted: 10 January 2024 / Published online: 24 January 2024
© The Author(s) 2024

Abstract

Despite the widespread use of fused filament fabrication (FFF) (an extrusion-based additive manufacturing process) to manufacture end-use parts for the aerospace industry, limited materials are available within this process that can be used for structural applications in the harsh space environment. Currently available high-performance polymers need to be improved by incorporating additives within the polymer matrix to achieve multi-functional properties. Additives such as graphene, graphene oxide, carbon nanotubes and boron carbide are known to improve mechanical and thermal properties and radiation shielding. This study aims to understand if these additives can be successfully incorporated into PEKK matrix to manufacture printable filaments for FFF. Graphene, graphene oxide (GO) and boron carbide (B_4C) were compatibilised with PEKK matrix, and their mechanical, thermal and rheological properties were analysed and compared with commercially available carbon fibre and carbon nanotube-reinforced PEKK where appropriate. As rheological properties of the formulations confirmed that they were printable, filaments for FFF were then manufactured. Graphene–PEKK was the most printable filament followed by GO–PEKK while B_4C –PEKK was not printable. TEM images of filament cross-section showed good dispersion of graphene and graphene oxide, while boron carbide formed large agglomerates; B_4C also presented feeding issues due to its hardness which affected its printability. Dispersion of the additives was also confirmed by studying their X-ray diffraction (XRD) patterns, and chemical structures were assessed using FT-IR spectroscopy. Finally, parts were printed using selected composite filaments, and their porosity and surface roughness were compared with neat PEKK and commercial CNT-reinforced PEKK to develop an understanding of metrology and bulk material properties of the composites.

Keywords Fused deposition modelling (FDM) · Nanocomposites · Rheology · Transmission electron microscopy (TEM) · X-ray diffraction spectroscopy · Porosity

1 Introduction

With a renewed global interest in space exploration, there is a demand for light-weight composite materials that can replace heavier metals and survive in the space environment. This is particularly challenging as material for space applications require specific properties such as low outgassing [1, 2], electrostatic dissipation [3, 4], excellent mechanical [5] and thermal [6] properties, thermal stability [7] and

radiation shielding properties [8, 9] due to varied environmental conditions in space [6].

Additive manufacturing (AM) is an advanced manufacturing technique that helps reduce the mass of structures by offering design topology optimisation and reducing joints and fixtures [10]. An AM process called fused filament fabrication (FFF) has been in the limelight of research for in space manufacturing [11–13]. In space manufacturing is particularly important for astronauts to manufacture tools and parts on demand during extended missions in space [14]. Most other AM techniques use powders or liquids as raw materials making them incompatible in vacuum environment, but FFF uses thermoplastic filaments and thus has the potential to be used for in space manufacturing [15]. In FFF process, a thermoplastic filament is heated above its melting temperature and extruded through a nozzle. The nozzle moves in the X – Y plane to form a single layer then the print

✉ Kaifur Rashed
kaifur.rashed@gmail.com

¹ Center for Additive Manufacturing, RMIT University, Carlton, VIC, Australia

² CSIRO Manufacturing, 20 Research Way, Clayton, VIC, Australia

bed moves in the *Z* plane to allow for subsequent layers to be added, thus forming a 3D structure [16]. Although FFF has been the subject of research studies that worked on in space manufacturing, there are limited materials available which are printable using the FFF process and can withstand prolonged exposure to the harsh space environment.

Thermoplastics such as polyetherimide (PEI) [17], polyether ether ketone (PEEK) [18, 19] and polyether ketone (PEKK) [1, 19] are being used to manufacture components for space. While all these polymers possess excellent thermal, mechanical, and outgassing properties, PEKK was of particular interest due to its relatively low melting temperature and slow crystallisation, making it more processable [20]. While PEKK possesses some of the properties required in space, e.g. excellent thermal and mechanical properties and low outgassing, other required properties such as electrostatic dissipation and radiation shielding can be achieved by reinforcing PEKK with nanofillers [21–23]. However, the properties of the printed components using nanocomposite filaments are largely dependent on factors such as the particle shape and size distribution [23–25], dispersion and agglomeration [23, 26] of the additives. PEKK is a copolymer which consists of a para substitution carbonyl group called terephthaloyl (T) and a meta substitution group called isophthaloyl (I), chemical structure of which is shown in Fig. 1 [20, 27–29]. Various commercially available grades of PEKK have different T/I ratios ranging from 60/40 to 80/20 [20]. The melting temperature of PEKK increases with an increase in T/I ratio, while glass transition temperatures remain unaffected [28]. Hence, PEKK grades with lower T/I ratio are more easily processable in the FFF process. As a result, PEKK with T/I ratio of 70/30 and 60/40 were initially selected for the current study.

The objectives of this study were to produce PEKK matrix composites for FFF by incorporating additives that can potentially yield composites for structural applications in space environment, and develop an understanding of structure–property relationship of these composites. While previous studies have mostly reinforced commodity and engineering thermoplastics to manufacture composite filaments for FFF, more limited studies have incorporated additives in high-performance polymers which is a barrier to

expand their applications as structural components. Three different additives were selected based on literature review, and the effects of these additives on properties such as thermal, chemical, mechanical, viscoelastic and microstructure were studied and compared. The distribution and dispersion of each of the additives were studied and benchmarked with commercial PEKK matrix composites. In addition, the printable filaments were identified and utilised to print small specimen, and their porosity and surface roughness were studied to develop an understanding of metrology and bulk material properties of the printed composites when compared to neat PEKK.

2 Literature review

Various properties of thermoplastics have been enhanced by introducing additives to the matrix in previous studies. For instance, shielding of neutrons for space applications is generally performed with boron-10 due to its large neutron cross-section [30]. ^{10}B isotope was found to be a safe and effective way to absorb neutrons as ^{10}B reacts with neutron to produce ^4He and ^7Li , both of which are not radioactive [31]. HDPE/ B_4C composites offered better radiation shielding efficiency than HDPE/ BN composites due to weak interfacial adhesion between HDPE and BN [32]. Boron nitride (BN) was also used in a study to improve the neutron absorption of ABS manufactured via FDM. Results showed that BN -ABS composites improved neutron attenuation by up to 21% with 20% of BN in ABS matrix. BN also improved the char yield of neat ABS but deteriorated mechanical properties of neat ABS [33]. Boron carbide is a commonly used material for shielding in nuclear reactors due to its neutron absorption ability [34]. Its high hardness makes it suitable as an abrasive, for cutting tools and high wear applications [35]. A recent study incorporated up to 30% of boron carbide into PEEK matrix for FFF. Results showed that the composites with only 100-mm-thick barriers could effectively absorb up to 88.24% of neutrons. Although mechanical properties were initially reduced due to B_4C , post print annealing improved flexural and tensile properties [36].

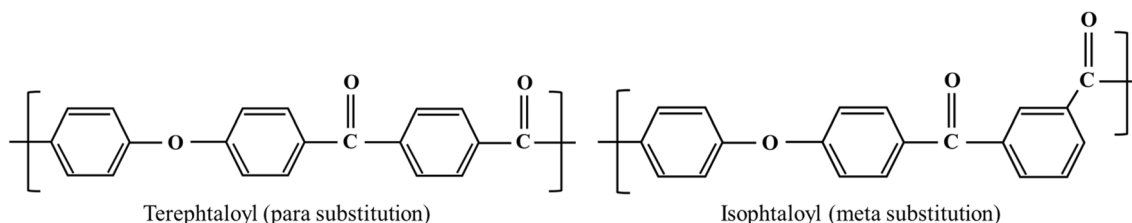


Fig. 1 Chemical structure of PEKK which consists of terephthaloyl and isophthaloyl isomers [29]

Graphene is classified as an exceptional filler material due to its high intrinsic thermal conductivity which aids with thermal management [37, 38], and its ability to bind with numerous matrix materials [39–42]. Moreover, graphene possesses many other properties which makes it attractive for use in materials for space, e.g. excellent electrical conductivity, mechanical strength and chemical resistance [43]. Graphene nanoplatelets (GNP) are extremely thin particles which consist of short stacks of 2D graphene sheets and possess superior electrical, mechanical and thermal properties [44]. Tambrallimath et al. performed thermal and mechanical characterisation of neat PC-ABS and filaments containing up to 0.8% of graphene. The results revealed an increase in Young's modulus and glass transition temperatures with the introduction of this carbon allotrope with 2D lattice structure [45]. Polyamide 12 reinforced with nanoplatelets of graphene showed similar results with optimum graphene content determined to be 6% [46]. Graphene also improved creep and wear resistance in PLA [47] but reduced impact strength [48]. Graphene nano platelets (GNP) were used to reinforce PEEK in a study which found that GNP reduced the coefficient of thermal expansion of PEEK substantially and thus improved the dimensional stability of the printed parts. The same study also reported that the tensile modulus of PEEK increased with increasing wt% of GNP and other properties such as electrical conductivity and storage modulus in the glassy region was improved due to the addition of GNP [49]. PEKK was also reinforced with graphene and carbon black in a study to improve the electrical conductivity of the neat polymer. The nanocomposites were mixed using a twin-screw extruder and results showed that graphene improved the dielectric permittivity of PEKK by 31 times while not affecting its mechanical properties [50].

Graphene oxide (GO), like graphene, has a 2D structure and is a single-atom carbon layer with both surfaces modified by functional groups which contains oxygen [51]. Graphene oxide (GO) and short carbon fibre were used to reinforce polyethersulfone (PES), improving the neat polymer's mechanical properties at cryogenic temperatures [52]. Graphene oxide was also used to reinforce medium-density polyethylene (MDPE) to manufacture structural components for space [53]. The study proved that compared to boron carbide (B_4C) and single-walled carbon nanotubes (SWCNT), graphene oxide provided better radiation protection when dispersed in MDPE. The shielding effectiveness of GO was due to the presence of functional groups such as epoxide, hydroxyl, carboxyl and carbonyl which enhances its hydrogen content [53].

Carbon nanotubes (CNT) are long and thin hollow nanomaterials comprised of single or multiple layers of rolled graphene [54]. Features of CNT such as excellent mechanical, electronic, optical and chemical characteristics make it suitable for numerous current and future applications [55,

56]. Polybutylene terephthalate (PBT) was reinforced with CNT and graphene, and the results showed that PBT/CNT had better conductive and mechanical properties than PBT/graphene structures due to the formation of agglomerates in PBT-graphene composites [23]. Continuous CNT yarn filaments were used to reinforce ULTEM (a polyetherimide-based thermoplastic supplied by SABIC [57]) in a study. The resulting composite material was used to manufacture a quadcopter frame. The CNT yarn also acted as electrical conductors carrying current to the motors [58]. CNT was used in another study to reinforce polyvinyl alcohol (PVA) where results showed that CNT increased the glass transition temperature and viscosity of the material and made the samples tougher while the ultimate mechanical properties were unaffected [59]. However, the presence of CNT in PEEK did not influence the mechanical properties of samples. CNT was used between 1 and 5%, and although cross-section of 5% CNT-PEEK showed signs of CNT being well dispersed, they had the lowest ultimate tensile strength [60].

Carbon fibres have been used in the form of short fibres [61] and continuous yarns [62] to reinforce various polymers for the FFF process. Continuous yarns of carbon fibres are beneficial in applications requiring improved mechanical performance [63], thermal [62] and electrical [64] conductivity. A recent study has also shown that continuous yarns of carbon fibres can be used to reinforce polyetherimide—a high-performance polymer [65]. However, studies have shown that high loading of carbon fibres can prove to be disadvantageous, e.g. adding up to 5 wt% carbon fibres in ABS matrix improved mechanical properties, while higher wt% resulted in increased porosity and thus deteriorated flexural and tensile properties [61]. Li et al. also studied the effects of short carbon fibre on FFF-printed PEEK in different build orientations. The study found that the addition of carbon fibres improved the uniform nucleation process of PEEK which increased its degree of crystallinity and hence enhanced flexural modulus. However, disadvantages of carbon fibres such as increased percentage and size of porosity and brittleness were also revealed [66].

Graphene, graphene oxide and boron carbide were used as additives in this study. These additives offer properties such as high electrical [67, 68] and thermal [53, 69] conductivity, excellent thermal [45, 46, 69], mechanical [45, 46, 52] and neutron shielding [53] properties while producing processable composites for FFF [36, 70]. These additives thus have the potential to expand the applications of FFF-printed PEKK to manufacture structural components for space environment.

3 Materials

Polyether ketone ketone (PEKK) pellets with a T/I ratio of 60/40 and 70/30 were acquired from Arkema with commercial name of Kepstan PEKK 6002 and 7002, respectively.

Thermal and viscoelastic properties of the two grades of PEKK were initially compared as discussed in SI-A, and PEKK with T/I ratio of 60/40 was selected as the matrix polymer for the composites. Sources and properties of the acquired additives for the composites are shown in Table 1. In addition, carbon nanotubes (CNT) and carbon fibre (CF) reinforced PEKK filaments were ordered from 3DX-Tech commercially known as ESD-PEKK and CF-PEKK respectively to benchmark the manufactured filaments.

4 Methodology

4.1 Thermogravimetric analysis (TGA)

Thermogravimetric analysis was conducted using Netzsch STA 449 in a nitrogen environment. Of PEKK and composites, ~20 mg samples were taken from pellets and loaded on to an aluminium pan. The samples were heated from ambient temperature to 167.3 °C at 10 °C/min. The samples were then dried at 167.3 °C for 20 min followed by a ramp rate of 10 °C/min to 1000 °C [71].

4.2 Differential Scanning Calorimetry (DSC)

TA Instruments DSC 250 was used in a modulated mode to conduct thermal characterisation of neat PEKK and composite pellets under nitrogen environment. The instrument was calibrated using a standard sapphire sample. All samples were heated from 25 to 400 °C then maintained isothermally at 400 °C for 3 min before cooling the samples to 25 °C. The samples were soaked at 25 °C for 3 min and then heated again to 400 °C. Heating and cooling were performed at a rate of 5 °C/min, and sample size was kept between 5 and 7 mg. Glass transition temperature, melting temperature and heat of fusion data were obtained from the 2nd heating cycle to remove the influence of any thermal history. Percentage crystallinity was calculated using the following formula [49]. Percentage crystallinity of commercial filaments could not be calculated as the mass fraction of PEKK could not be determined.

$$X_c = \frac{\Delta H_c}{w\Delta H_c^o} \times 100\%$$

Where

X_c % crystallinity

ΔH_c Enthalpy of crystallisation in J/g

w mass fraction of PEKK in the composites (1.0 for neat PEKK)

ΔH_c^o Enthalpy of crystallisation of 100% crystalline PEKK, assumed to be 130 J/g [72]

4.3 Rheology

The neat PEKK and composite pellets were used to manufacture compression moulded rheology discs with 25 mm diameter and 2 mm thickness. The pellets were filled in a mould which was heated to 340 °C and pressed at a pressure of 10 kPa for 5 min followed by cooling under pressure for 5 min. PTFE sheets were used on both sides of the mould to ensure easy release. The rheology of neat PEKK and composites was analysed using a Discovery HR 3 rheometer. Twenty-five millimetre parallel plate geometry was used for all experiments, and the discs were dried overnight at 120 °C to remove any moisture. All analysis was performed between 360 and 390 °C at 10 °C intervals. The gap between the plates was kept consistent at 1000 µm. Initially, strain amplitude sweep tests were performed between oscillation strain of 0.1 to 100% at a constant frequency of 10 rad/s to determine the linear viscoelastic region (LVR) of the materials [73, 74].

Subsequently, a frequency sweep test was performed between 0.1 and 628 rad/s by applying a constant oscillation strain within the LVR [73, 74]. This was done to determine the variation of loss modulus, storage modulus and complex viscosity with angular frequency. The same analysis was repeated on commercially available carbon fibre and carbon nanotube-reinforced PEKK. The commercial filaments were initially pelletised to manufacture the compression moulded samples.

4.4 Melt compounding and filament manufacturing

Pellets of 60/40 PEKK were used to manufacture neat PEKK filaments using a single-screw extruder. Previous studies illustrated methods to manufacture filaments using polyamide 6 [75], ULTEM 1010 [76] and PEEK [49], all of which included a water bath to cool the filament after extrusion, and hence a similar method was implemented for this study initially. However, visible air bubbles appeared within the filament after water cooling as shown in Fig. 2. The method

Table 1 Sources and properties of additives used in the current study

Additive	Manufacturer	Country of origin	Purity (wt.%)	Diameter (µm)	Thickness (nm)
Boron carbide	Sigma-Aldrich	Germany	98	<74	-
Graphene	XF NANO	China	99	2–7	2–6
Graphene oxide	XF NANO	China	>97	~20	≤5

was then modified to cool the filaments using an air curtain as illustrated in Fig. 3, resulting in filaments without any visible air bubble. To manufacture composite pellets, PEKK pellets and additives were first weighed and mixed in a zip lock bag. The mixtures were then fed into a Haake twin-screw extruder with 25-mm co-rotating screws, and the filaments were cooled using a conveyer belt and then fed into a pelletiser.



Fig. 2 Filaments cooled using water bath (trial 1) and air curtain (trial 2)

The pellets were also used to manufacture filaments for FFF printers with 1.75 ± 0.1 mm diameter using a Haake™ Rheomax single-screw extruder fitted with a 2-mm die. Schematic of the entire process is shown in Fig. 3. A typical configuration of a single-screw extruder with heating zones identified is shown in Fig. 4, and the extrusion conditions for each formulation are displayed in Table 2. Note that extrusion conditions for all the composites were the same except for 1% GO–PEKK which was extruded at a lower temperature due to its lower viscosity which produced filaments that were mostly flat and not cylindrical as required in FFF printers. A micrometre screw gauge was used to take measurements of filament diameter periodically during the extrusion process.

4.5 Flexural test

Specimens for flexural tests were manufactured using DSM Micro 15 injection moulding machine. The cylinder temperature of 350 °C and mould temperature of 170 °C were kept consistent for all samples. A screw speed of 35 rpm was used for neat PEKK and 50 rpm was used for the composites. Three-point bend tests were performed on the injection moulded samples using Instron 5900 as per ASTM D 790 – 03 [77] to determine the flexural properties of neat and reinforced polymers. Three to six specimens from each sample groups were used for the analysis. All specimens were conditioned in a lab environment for 48 h before testing. Testing parameters were

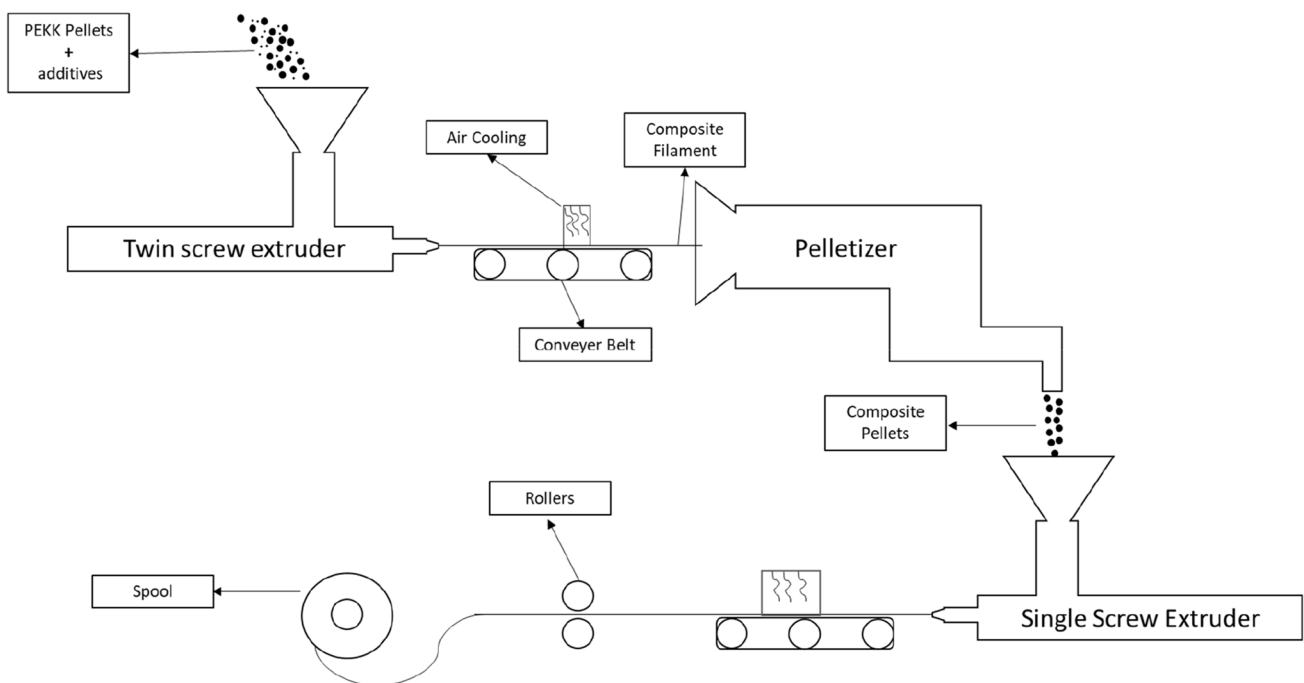


Fig. 3 Schematic of extrusion process for composite pellets and filament manufacturing

Fig. 4 Typical configuration of a single-screw extruder with heating zones identified

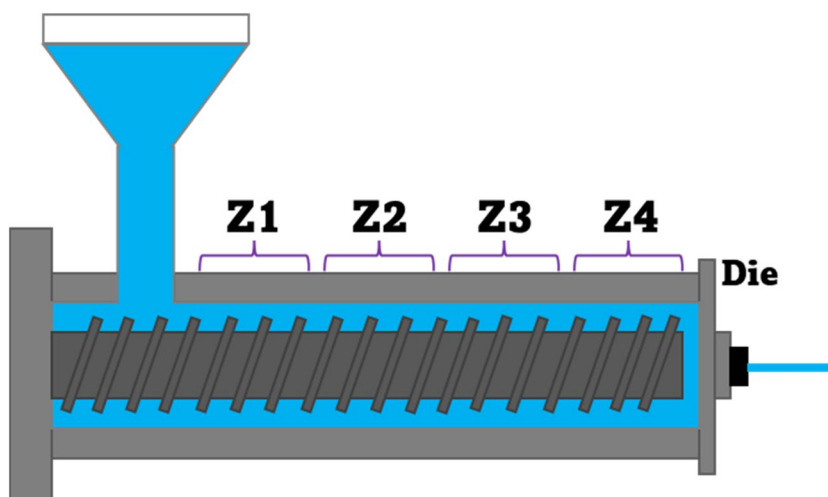


Table 2 Extrusion conditions for manufacturing filaments for each formulation

Formulation	Zone 1 (°C)	Zone 2 (°C)	Zone 3 (°C)	Zone 4 (°C)	Extruder speed (rpm)
Neat PEKK	280	290	290	290	30
1% B ₄ C	290	300	300	300	40
5% B ₄ C	290	300	300	300	40
1% graphene	290	300	300	300	40
5% graphene	290	300	300	300	40
1% GO	280	290	290	290	40
5% GO	290	300	300	300	40

kept consistent throughout, e.g. span width of 64 mm and rate of displacement of 1.71 mm/min.

4.6 Filament morphology

Cross-sections of the composite filaments were microtomed using a diamond knife to achieve samples with thickness of 50–80 nm. The cross-sections were then analysed under a transmission electron microscope (TEM) to study the dispersion and distribution of additives. As we experienced challenges with microtoming the B₄C-reinforced filament due to its hardness, this filament was dipped in liquid nitrogen and then fractured; the fracture surface was then observed under a Zeiss Merlin FE SEM equipped with 100 mm² Oxford Extreme SSD detector. Curved surfaces of the filaments were imaged using a FEI Quanta Scanning Electron Microscope (SEM) after coating with iridium. A voltage of 30 kV, spot size of 5 and working distance of ~10 mm were kept consistent for all samples.

4.7 X-ray diffraction (XRD) spectroscopy

XRD spectroscopy was performed on graphene, graphene oxide and boron carbide powders and compression moulded neat PEKK and the composites using Bruker D4 Endeavor XRD. Consistent parameters used for all experiments were step size of 0.02°, divergent slit v6, voltage 40 kV and current 35 mA. Background subtracted spectra for each sample were reported and compared to identify differences in the crystalline structure of PEKK due to the additives.

4.8 FFF manufacturing

Samples were manufactured using neat PEKK and composite filaments by a custom-built FFF printer equipped with a heated bed and no heated chamber. No visible deformations were observed in the printed components after printing. Our previous study which optimised the process parameters to minimise the porosity of PEKK found that linear infill pattern, 8 contours, 0°/90° raster angle produced parts with minimum porosity in the printer used for this study [78].

Table 3 Consistent process parameters used for all prints

Parameter	Magnitude
Nozzle size (mm)	0.4
Bed temperature (°C)	120
Layer height (mm)	0.1
Print speed (mm/s)	20
Infill density (%)	100

Table 4 Process parameters that were varied for each material

Material	Print temperature (°C)	Flow (%)
Neat PEKK	360	100
1% GO	350	90
1% graphene	360	100
5% graphene	360	100
CNT PEKK	370	100

Thus, the optimized process parameters were kept consistent for all prints. Other consistent parameters are displayed in Table 3 while Table 4 lists the process parameters that were varied for each material.

4.9 Electrical conductivity

The electrical conductivity of specimens was measured using a custom-built probe connected to a digital multi-metre. Resistance of the materials was determined using the multi-metre, and electrical conductivity was determined using the following equation [79].

$$\sigma = \frac{L}{RA}$$

Where

σ Conductivity in S/cm

L Length of conductor in cm

R Resistance of conductor in Ω

A Area of conductor cross-section in cm^2

4.10 Porosity analysis

The porosity of 10-mm cube samples was analysed using Bruker Skyscan X-Ray Micro Computed Tomography (μ -CT). The number of frames used for the analysis was kept consistent in all samples to ensure results are consistent between specimens. Scans were completed using no filter with a voltage of 40 kV and a current of 175 μA . Pixel size was kept consistent at 8.5 μm for all samples, and a beam hardening correction of 5% was used. Images of cross-sections were captured using NREcon software, porosity was determined using CTan software and pores within the samples were visualised using CTVox software.

In addition, sphericity and size of pores were obtained from CTan software, and plots of sphericity vs size of pores were reported for each printed sample.

4.11 Surface roughness

3D profiles of the top and side surfaces of printed samples were obtained using KLA Tencor P16 + contact system profilometer with a tip radius of 2 μm . Scan size 200 \times 200 μm , scan speed 5 $\mu\text{m/s}$, sampling rate 50 Hz and applied force of 0.5 mg were kept consistent for all samples. 3D profiles and average roughness, R_a , for each surface were reported.

5 Results and discussion

5.1 Thermal analysis of composites

5.1.1 Thermogravimetric analysis (TGA)

Thermogravimetry curves of PEKK and the composites are shown in Fig. 5. With the application of linear heating in an inert environment, PEKK and its composites show two steps of heat loss. The first step, within temperatures of 500–650 $^{\circ}\text{C}$, is the major decomposition step as most of the material volatilises within this temperature [80]. At this stage, thermal decomposition promotes the formation of a crosslinked structure [81]. Owing to the formation of a more thermally stable structure, the rate of weight loss reduces around 700 $^{\circ}\text{C}$. Upon further heating, the crosslinked structure decomposes and yields a thermally stable char [81]. Decomposition onset temperature (DOT) and char yield were parameters used to draw comparisons between the thermal decomposition behaviour of the formulations. Decomposition onset temperature is considered the temperature at which the material loses 1% mass [73], and char yield is defined as the percentage of initial mass remaining at 1000 $^{\circ}\text{C}$ [82].

All additives influenced the decomposition onset temperature and char yield of PEKK (Fig. 5). Onset of decomposition occurred at a lower temperature, and char yield was increased due to the additives. However, the decomposition onset temperature was above 500 $^{\circ}\text{C}$ for all formulations, which indicates the upper limit of polymer processing temperature. A lower decomposition onset temperature is typical in polymer matrices containing intumescent compounds [76, 83] such as graphene [84], graphene oxide [85] and boron carbide [86] which may indicate that the additives interfere with the natural thermal degradation process of PEKK [87]. An increase in char yield of the composites can be attributed to strong barrier properties of the additives, shielding the matrix polymer from external heat flux, and reducing mass transport from PEKK [87]. Char yield was highest in CNT-reinforced

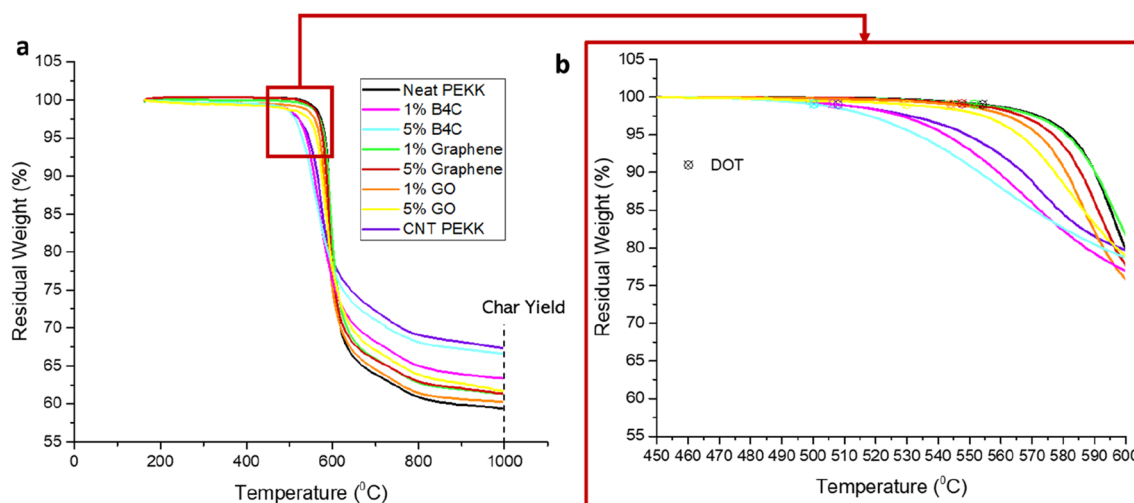


Fig. 5 TGA of PEKK and composites (a) full temperature range with char yield identified and (b) between 450 and 600 °C with decomposition onset temperature (DOT) identified

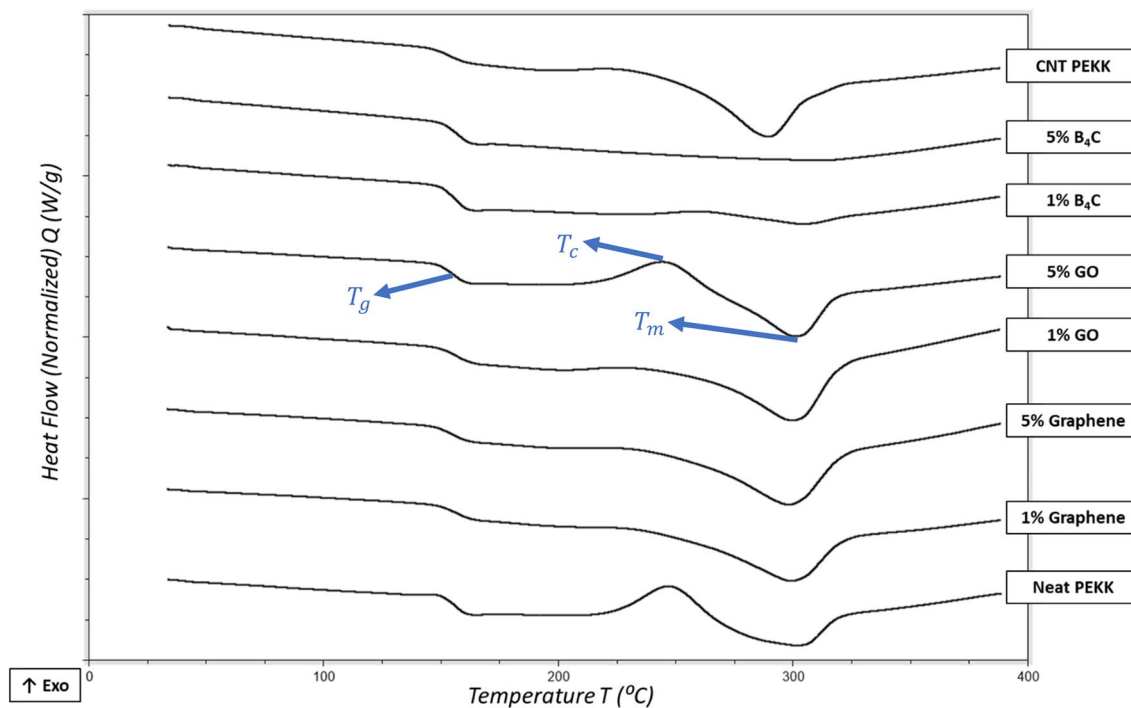


Fig. 6 DSC 2nd heating curves of PEKK and composites

PEKK (possibly due to high loading of additives) followed by 5% B₄C-reinforced PEKK. Increasing loading of GO and B₄C brought noticeable improvement in char yield, whereas increasing loading of graphene did not significantly affect char yield. The decomposition behaviour of 1% and 5% graphene-reinforced PEKK was very similar. The increased char yield of B₄C-reinforced PEKK can be attributed to the high thermal stability of B₄C due to its

inorganic nature [76] and oxidation of B₄C and production of solid amorphous carbon [88].

5.1.2 Differential scanning calorimetry (DSC)

Figure 6 shows the 2nd heating curves for each formulation as obtained from DSC analysis. Upon heating from room temperature in nitrogen environment, neat PEKK

experienced a glass transition between 147 and 163 °C, followed by cold crystallisation between 220 and 263 °C and finally melting between 263 and 321 °C. The temperature corresponding to the midpoint of the glass transition region was considered glass transition temperature, and temperatures corresponding to the peak of cold crystallisation and melting regions were considered cold crystallisation and melting temperatures respectively as shown in Fig. 6. Glass transition temperatures of all formulations were between 151 and 156 °C. Neat PEKK experienced cold crystallisation with a peak at 245 °C which was minimised for most other formulations except 5% graphene oxide. Similar observations were reported when graphene nanoplatelets were compatibilised with PLA/TPS in another study [89]. Graphene nano platelets and graphene oxide act as nucleating agents and facilitate the crystallisation of PEKK [89]. This is further confirmed by analysing the cooling curves.

Figure 7 shows the overlay of cooling curves from DSC (between 290 and 190 °C) for each formulation, and Table 5

lists the key thermal properties of all the formulations determined from TGA and DSC analyses. While cooling from melt, neat PEKK did not experience any transition, which indicates that PEKK was initially mostly amorphous, and the degree of crystallinity increased by up to 19% due to the nucleation effect of graphene and graphene oxide [89, 90]. The temperature and degree of crystallinity of neat PEKK increased due to all the additives except boron carbide, possibly due to the size of the boron carbide particle used. This indicates that except boron carbide, all other additives were uniformly dispersed within the polymer matrix [49] as adding nanoparticles within polymer matrix generally increases T_c due to their nucleating effect [90]. Pedoto et al. showed that an increase in the degree of crystallinity increases the elastic modulus of PEKK [91]. However, the degree of crystallinity of 5% graphene oxide-reinforced PEKK was significantly lower than 1% graphene oxide-reinforced PEKK possibly due to the formation of some agglomerates. The effective contact surface area between

Fig. 7 DSC cooling curves of PEKK and composites

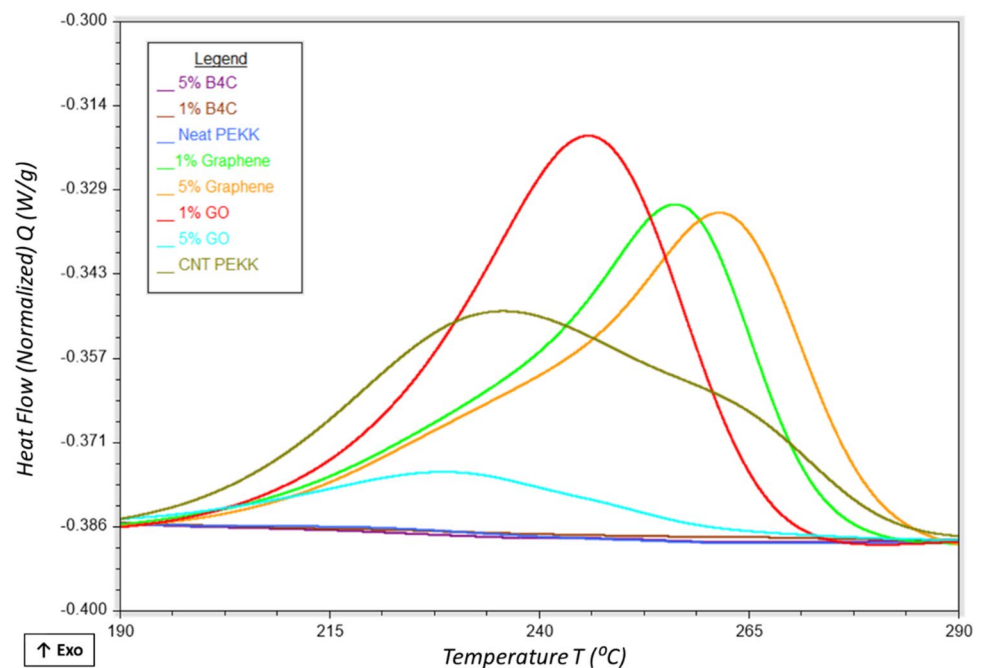


Table 5 Key thermal properties of PEKK and composites from DSC and TGA

Material	T_g (°C)	T_m (°C)	T_c (°C)	X_c (%)	DOT (°C)	Char yield (%)
Neat PEKK	155.1 ± 0.5	302.5 ± 0.6	221.4 ± 1.7	0.28 ± 0.12	555.5 ± 1.2	58.58 ± 0.07
1% B ₄ C	155.3 ± 0.4	305.2 ± 0.9	222.7 ± 0.1	0.01 ± 0.00	522.4 ± 2.2	66.15 ± 0.20
5% B ₄ C	155.9 ± 0.1	313.2 ± 1.7	216.3 ± 0.4	0.05 ± 0.01	493.4 ± 6.4	66.98 ± 0.30
1% graphene	155.2 ± 0.4	299.6 ± 0.5	256.4 ± 0.1	18.52 ± 2.31	554.5 ± 3.7	62.89 ± 1.58
5% graphene	154.3 ± 0.1	298.3 ± 0.2	261.6 ± 0.0	19.26 ± 1.34	546.0 ± 1.5	60.95 ± 0.42
1% GO	156.0 ± 0.1	300.5 ± 0.2	243.8 ± 2.0	18.80 ± 0.22	530.1 ± 0.8	58.62 ± 0.79
5% GO	154.3 ± 0.1	300.7 ± 0.4	228.7 ± 0.3	3.35 ± 0.02	515.9 ± 1.3	61.17 ± 1.04
CNT PEKK	151.8 ± 1.5	289.8 ± 0.3	236.3 ± 0.5	-	493.8 ± 2.3	66.45 ± 0.07

the additives and matrix polymer is generally reduced due to agglomeration [49]. Wang et al. reported similar observations when PLLA was reinforced with GO; the study found that the temperature and degree of crystallinity of the composites first increased then reduced with increasing loading of GO, with a maximum observed at 1% GO [92].

5.2 Rheology of composites

Supplementary Information B (Fig. B1 to B10) shows the strain amplitude sweep test results for PEKK and the composites. All the materials exhibit linear response up to a critical strain value, beyond which the storage modulus drops, indicating structural breakdown of the polymer [73, 93]. The introduction of the additives reduced the critical strain value beyond which the dynamic moduli were unaffected, CNT-PEKK most significantly. This suggests that loading of additives in CNT-PEKK filaments was higher than in all other formulations examined [73]. Figure 8 shows the complex viscosity plots for all the formulations. Most formulations displayed relatively Newtonian behaviour at low frequencies (< 1 rad/s) and shear thinning at frequencies higher than 1 rad/s except for 5% GO-PEKK and CNT-PEKK which displayed shear thinning behaviour across all frequencies. The shear thinning effect was most prominent in CNT-PEKK which suggests that CNT interacted strongly with the PEKK matrix, interfering with the relaxation process of PEKK macromolecules, hindering their complete relaxation [94]. A closer look at the viscosity values within the FFF range (Fig. 8(b)) of 100 to 200 rad/s [73] shows that all manufactured formulations had viscosity lower than commercial CNT and CF reinforced PEKK within this range and thus in theory, all formulations are printable.

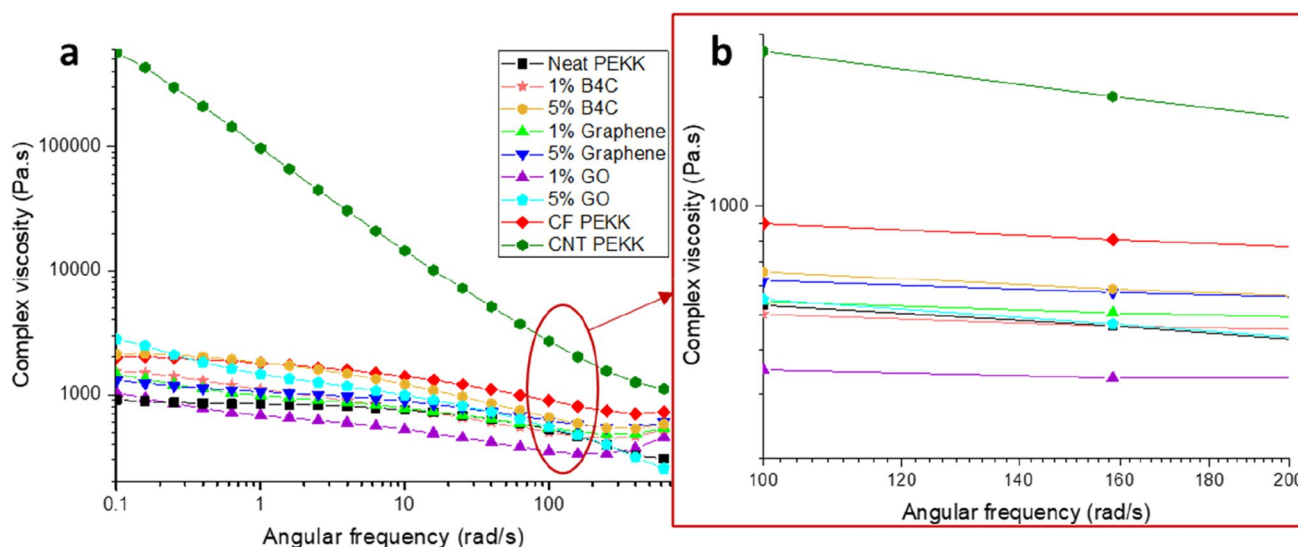


Fig. 8 Rheology of PEKK, developed and commercial composites in full angular frequency range (a) and partial range of 100 to 200 rad/s (b)

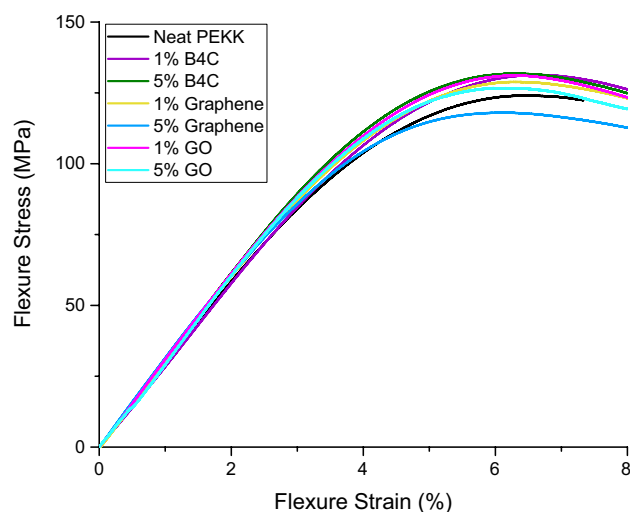


Fig. 9 Flexure properties of PEKK and composite formulations (representative specimen from each formulation)

Dynamic modulus vs angular frequency plots (Fig. C1 to C10 in SI C) show that loss modulus (G'') was higher than storage modulus (G') across most frequencies and all temperatures for all the formulations except neat PEKK and 5% GO-PEKK at 390 °C. A higher G' indicates that the elastic component of the material dominates the viscous component, and thus a higher G' is favourable in FFF to ensure printed parts can retain their shape [73, 95]. Hence, the printing temperature of neat PEKK and 5% GO-PEKK filaments should be restricted to 380 °C to maximise dimensional accuracy.

5.3 Flexure test

Figure 9 shows the flexure stress vs strain graphs of representative specimen from each formulation, and Table 6 lists the mean flexural modulus and flexural yield strength and their standard deviations. All the additives improved the flexural modulus of PEKK, whereas flexural yield strength was mostly unaffected due to the additives, except for 5% graphene, which reduced the yield strength of PEKK by 4.9%. Similar observations were reported in a study that reinforced PEEK with 5 wt% short carbon fibre where flexural modulus increased by 8.3%, but yield strength was unaffected [66]. The increase in flexural modulus of the composites can be attributed to the superior mechanical properties of boron carbide [96], graphene [97] and graphene oxide [98] than neat PEKK. The variation in flexural modulus (E) among the composites (i.e. $E_{\text{Graphene-PEKK}} > E_{\text{GO-PEKK}} > E_{\text{B}_4\text{C-PEKK}}$) can be attributed to the dispersion and distribution of additive within the polymer matrix. Studies have identified that the dispersion state of additives within a polymer matrix and interfacial strength between additives and matrix govern the mechanical properties of composites [49].

5.4 Filament morphology

Table 7 shows the mean diameter of the manufactured filaments, and Fig. 10 shows the images of the filaments. The dimensions of neat PEKK filaments were most suited for the custom-built printer which requires filaments with a diameter of 1.75 ± 0.10 mm. A stable dimension of filaments is important to ensure printability in FFF as inconsistencies in filament diameter can cause nozzle clogging, under-extrusion and as a result, affect the quality of printed parts [99, 100]. As the extruder used to manufacture filaments did not have any measures to control dimensions such as vacuum-assisted sizing [101], the diameter of the composites varied significantly which affected their printability. Both B_4C -reinforced PEKK and 5% GO-PEKK were not printable due to their large diameter, despite several attempts

using various process parameters. The larger diameter of these composites could be due to formation of agglomerates, which can be confirmed by studying microscopic images of cross section of the filaments.

Filament cross sections of developed composites with 5% loading and commercial CNT-PEKK were investigated using a transmission electron microscope (TEM) (Fig. 11). The 5% graphene filaments were relatively easier to microtome than the other samples. Five percent graphene oxide produced thick samples due to its hardness, and 5% boron carbide was extremely hard for the diamond knife, and only fragments of the cross section were obtained during microtoming. Cryo-fractured surface of the boron carbide reinforced PEKK was thus analysed under an SEM using EDS.

Graphene showed signs of intercalation and was well dispersed in the PEKK matrix. Graphene oxide also showed some intercalation. Some large agglomerates were present in graphene oxide samples. Boron carbide, however, formed large agglomerates, possibly due to the size of B_4C particle used [102], which may have contributed to reduced flexural properties of B_4C -PEKK samples as observed in Sect. 5.3. It

Table 7 Mean diameter of filaments from each formulation and their standard deviations

Formulation	Filament diameter (mm)
Neat PEKK	1.75 ± 0.05
1% B_4C	1.96 ± 0.06
5% B_4C	1.88 ± 0.07
1% graphene	1.85 ± 0.02
5% graphene	1.81 ± 0.05
1% GO	1.84 ± 0.05
5% GO	2.06 ± 0.10

Table 6 Key flexural properties of PEKK and composites (statistically significant results identified within brackets)

Formulation	Mean flexural modulus (MPa)	St Dev	Mean flexural yield strength (MPa)	St Dev
100% PEKK	2976.6	81.34	127.16	4.00
1% B_4C	3001.9	50.62	131.59	0.15
5% B_4C	3131.9 (+5.2%)	52.71	131.66	1.27
1% graphene	3127.6 (+5.1%)	16.19	131.59	2.59
5% graphene	3217.8 (+8.1%)	84.43	120.89 (−4.9%)	1.82
1% GO	3121.2 (+4.9%)	47.93	130.76	0.36
5% GO	3188.9 (+7.1%)	42.48	126.74	0.41

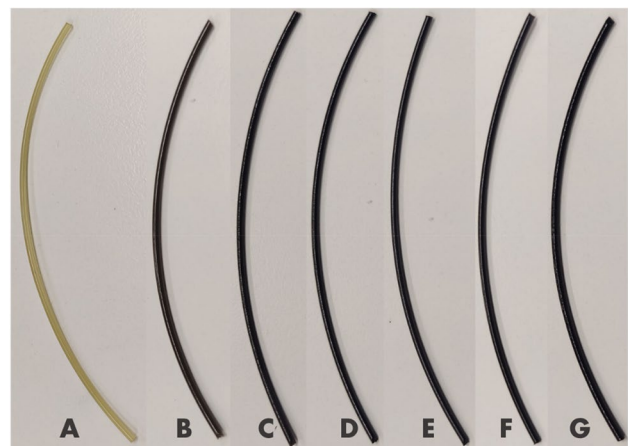


Fig. 10 Images of filaments manufactured using (A) Neat PEKK, and PEKK reinforced with (B) 1% B_4C , (C) 5% B_4C , (D) 1% graphene, (E) 5% graphene, (F) 1% GO and (G) 5% GO

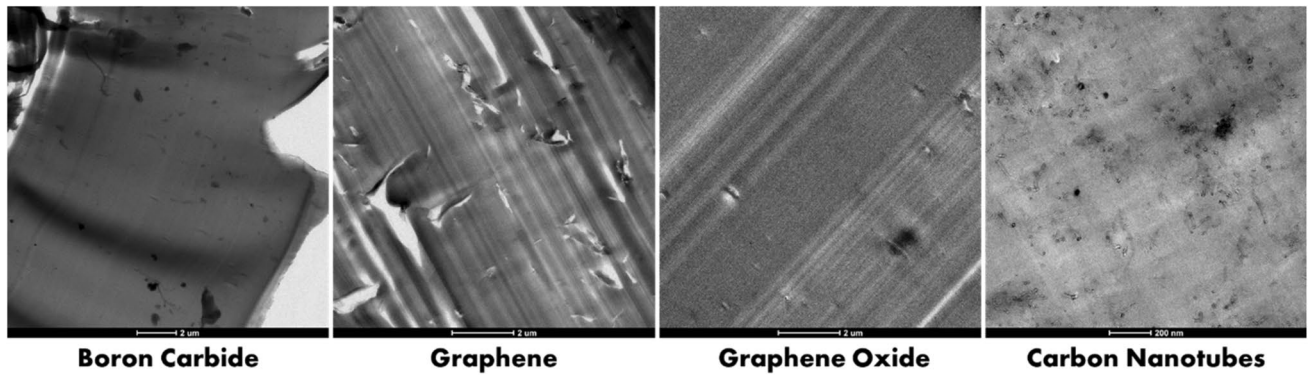


Fig. 11 TEM images of cross section of composite filaments

is particularly important to avoid the agglomeration of additives to achieve more homogenous properties throughout the composites and improve mechanical properties [103].

Figures 12 and 13 show the analysis on cross-section of cryo-fractured B_4C -PEKK filament. Figure 12 shows that the filament was quite porous and contained pores with a diameter between 30 and 100 μm . Pores are formed during the extrusion process due to factors such as entrapped pores during extrusion or formation of pores during cooling after extrusion due to thermal gradients that instigate residual stresses [104]. Figure 13 shows a large agglomerate of boron carbide, as identified from elemental analysis (Fig. 13(d)), such agglomerates may have contributed to partial fracture during microtoming. Previous studies have reported coating mechanisms to improve the dispersion and distribution

of B_4C in epoxy matrix [105, 106]. Surface treatment was also reported to improve the dispersion of boron nitride in HDPE [32] and B_4C in polyimide matrix [107]. Such surface treatment may improve dispersion and reduce agglomerates of B_4C in PEKK matrix. Moreover, reduced agglomerates and improved dispersion can also be achieved by using nano-sized B_4C instead [102].

Figure 14 shows the curved surfaces of the manufactured filaments compared to commercial PEKK-based composite filaments. All the manufactured filaments showed some signs of defects which can be attributed to residue from other polymers processed in the same extruder. Large bumps were present on the surface of B_4C -PEKK filament due to B_4C agglomerates which can significantly affect its printability. As B_4C possess high hardness [35], agglomerated

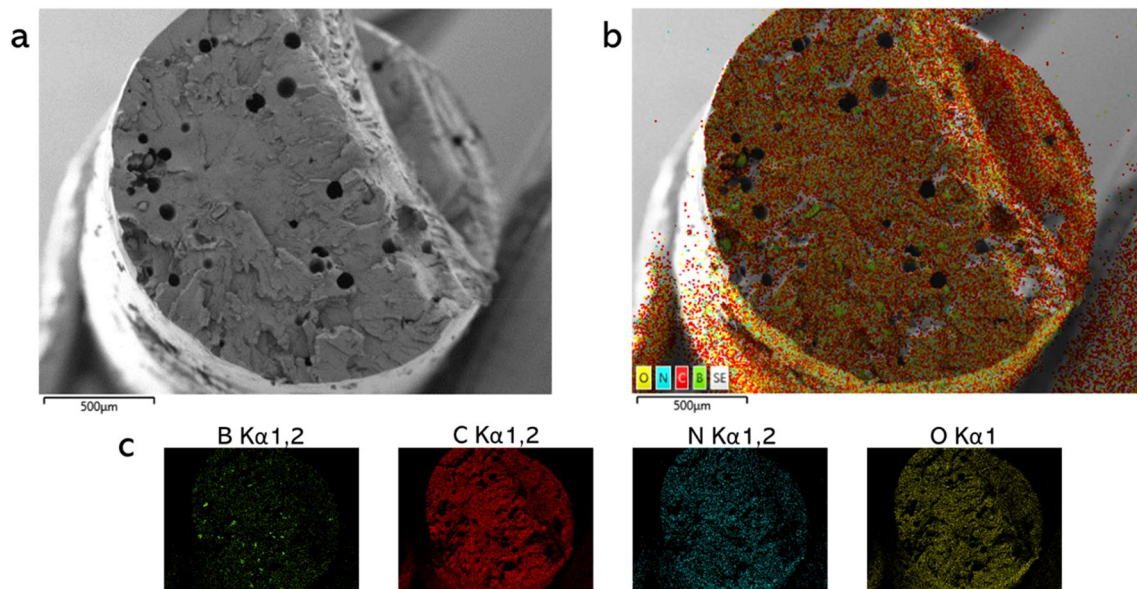


Fig. 12 Analysis on cross-section of B_4C -PEKK filament **a** SEM image of cross-section with 50 \times magnification, **b** EDS layered image, **c** elemental maps of boron, carbon, nitrogen and oxygen

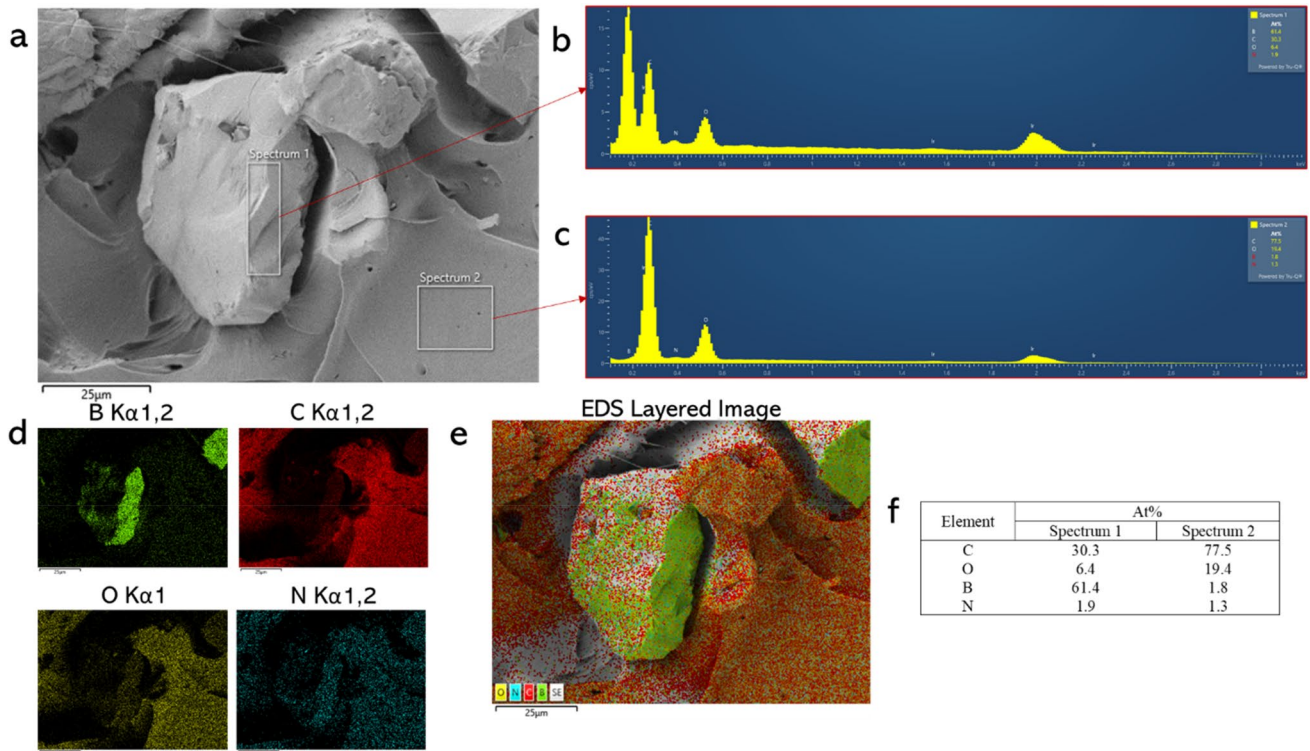


Fig. 13 Analysis on cross-section of B4C-PEKK filament (a) SEM image of cross-section with 1000× magnification, (b) and (c) EDS spectra from position identified in (a), (d) elemental maps of boron, carbon, oxygen and nitrogen, (e) EDS layered image and (f) elem

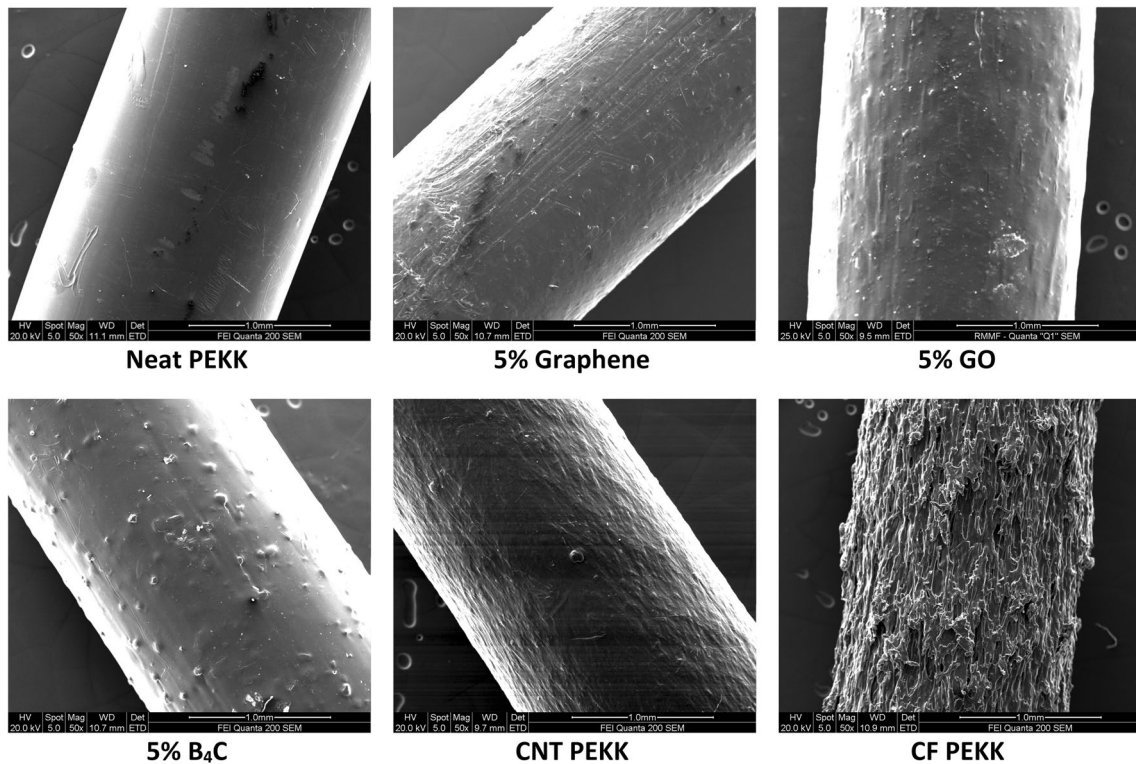


Fig. 14 SEM images of PEKK and developed composites compared to commercial filaments

B₄C particles on the surface can cause degradation of rollers (drive wheels) used for filament feeding in FFF printers, which are generally manufactured using steel. This further highlights the need to reduce agglomeration of B₄C particles to manufacture B₄C-based composites for FFF printers. The rough surface of CF-PEKK filament was possibly due to the morphology of carbon fibres [108].

5.5 X-ray diffraction (XRD) spectroscopy

Wide-range XRD patterns of all the composites compared to their raw materials (neat PEKK and additive powders) are shown in Fig. E1, E2, and E3 (SI E). The major characteristic peaks of PEKK crystalline structure were observed between 2 θ values of 12 to 32, which was unaffected due to the additives. For B₄C and graphene-based composites, the diffraction patterns were dependent on the wt% of additives. Consequently, GO did not influence the diffraction pattern of PEKK as evident in the spectra obtained from GO-based composites (Fig. E3) which is either due to weak characteristic peaks of pure GO or exfoliation and individual dispersion of GO in PEKK matrix [109]. The major characteristic peak for graphene nanoplatelets was observed at 26.5°, which was also present in the composites (Fig. E2), and intensity of this peak increased with wt% of graphene. This indicates that a high percentage of graphene nanoplatelets were intercalated in PEKK matrix [110], which is also confirmed by the TEM images of graphene–PEKK composite.

5.6 Electrical conductivity

Electrical conductivity of neat PEKK, formulated composites and commercial composites (CNT and CF reinforced PEKK) were measured. Of all the examined samples, only CNT-reinforced PEKK, commercially known as 3DX Tech ESD-PEKK, was conductive, while all other samples were nonconductive (measured resistance was zero). Possibly, the loading of fillers was not sufficient to form a percolating network or due to factors such as contact resistance and resin thick layer on the surface. Hence, to achieve electro-

static dissipation properties, either materials can be manufactured with higher loading of additives or post processing techniques such as electrodeposition can be utilised to coat the printed parts with a metal to provide surface conductivity [111, 112]. With a purpose to develop a comparison, both compression moulded and printed samples of CNT-reinforced PEKK were analysed. Compression moulded samples had a conductivity between 2.17×10^{-4} and 3.11×10^{-3} S/cm, and printed samples had a conductivity between 2.25×10^{-6} and 7.76×10^{-5} S/cm. The average conductivity of printed samples was roughly 100 times lower than compression moulded samples. The difference could be due to factors such as increased porosity [113] and existence of contact resistance between deposited filaments [114] in printed samples that reduces conductivity, and reduction of interparticle distance in compression moulded samples owing to the mechanical pressing action which improves conductivity in moulded samples [115].

5.7 Porosity analysis

The printable filaments (identified in Sect. 5.4) were used to print 10-mm cube samples (Fig. 15), and their porosity was studied using X-ray μ -CT. Figure F1 (SI-F) shows 2D cross sections of the samples at different heights from the build plate. All the samples showed signs of gradual increase in size and number of pores with height. The gap between contours was more prominent with height in neat PEKK, 5% graphene and CNT–PEKK samples.

Mechanical properties of FFF-printed parts [116] and their performance in vacuum environment [117] are considerably dependent on porosity within the parts, with low porosities preferred to maximise performance in high vacuum environment such as space. Previous studies have also proved that the mechanical performance of FFF-manufactured parts depends not only on the percentage of porosity, but also on location [118], shape [119] and size [119, 120] distribution of the pores within printed parts. Table 8 shows the percentage porosity, mean sphericity and mean diameter of pores within each printed sample. The sphericity

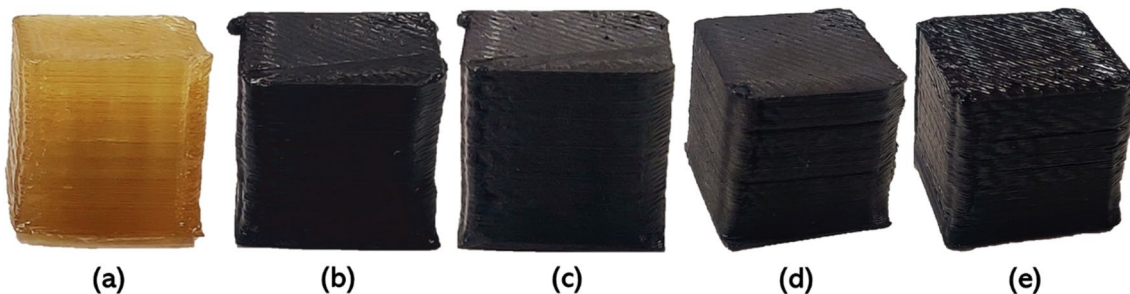


Fig. 15 Representative 10-mm cube samples printed using **a** neat PEKK, **b** 1% graphene oxide, **c** 1% graphene, **d** 5% graphene, and **e** CNT-PEKK

Table 8 Percentage porosity, average sphericity of pores and average diameter of pores determined from analysis of micro CT images

Sample	Porosity (%)	Mean sphericity	Mean diameter (mm)
Neat PEKK	0.68	0.81	0.091
1% GO	0.33	0.85	0.080
1% graphene	0.74	0.85	0.084
5% graphene	0.67	0.82	0.084
CNT-PEKK	0.60	0.81	0.093

of the pores measures how spherical the pores are; a pore with a perfectly spherical shape would have a sphericity of 1 [121]. The percentage of porosity within samples was similar except for 1% GO-PEKK which had lower porosity in comparison. The low porosity of 1% GO-PEKK could

be attributed to the material’s lower viscosity which caused over extrusion. The mean porosity of all the samples was similar, and hence pore morphology was further characterised by plotting the sphericity of pores vs size of pores [122] as shown in Figs. 16, 17, 18, 19 and 20. The average major diameter of pores was similar for neat PEKK and CNT-PEKK but slightly lower for the developed composites. The neat PEKK sample had 11 pores with diameter between 1 and 2 mm, which were reduced to 2 in 1% GO and CNT-PEKK samples and 0 in both graphene-PEKK samples. Mechanical properties of parts printed using the composites are thus expected to be superior to neat PEKK. In general, larger pores seem to have lower sphericity and thus can cause stress concentrations resulting in the failure of printed parts.

Images of pores within samples show that 5% graphene-PEKK sample possessed the most uniform

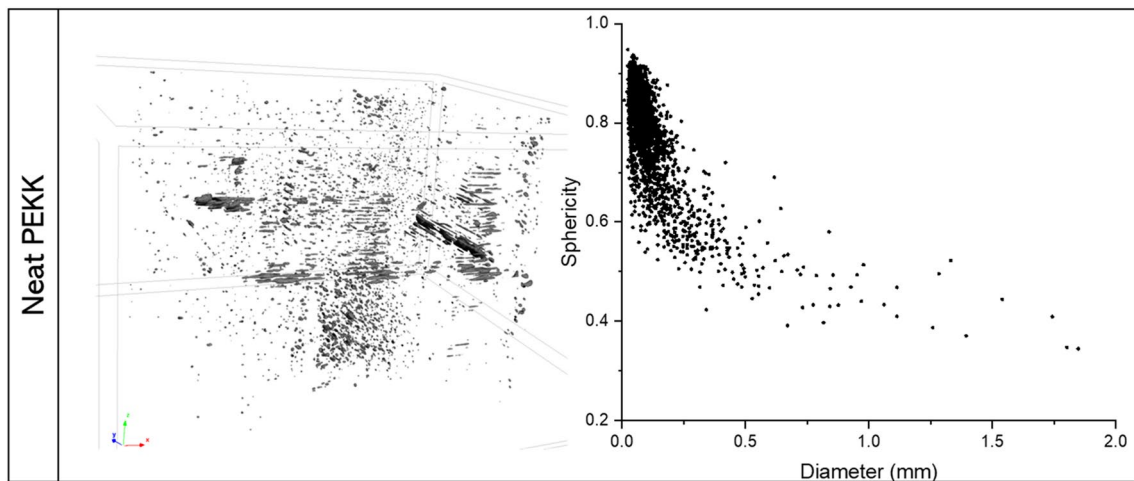


Fig. 16 Visual representation of distribution of 3D pores within Neat PEKK (left) and major diameter vs sphericity plot (right)

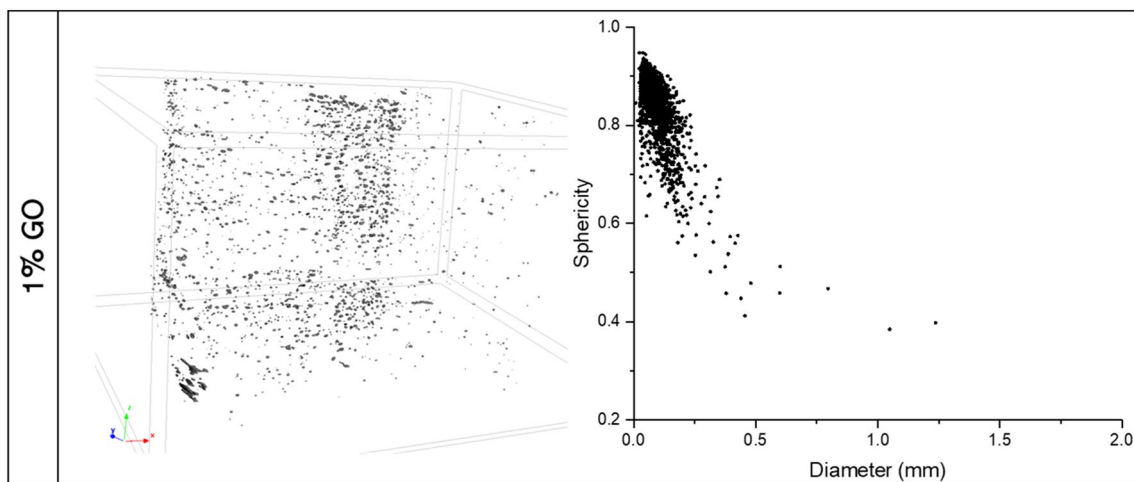


Fig. 17 Visual representation of distribution of 3D pores within 1% GO-PEKK (left) and plot of major diameter vs sphericity of pores (right)

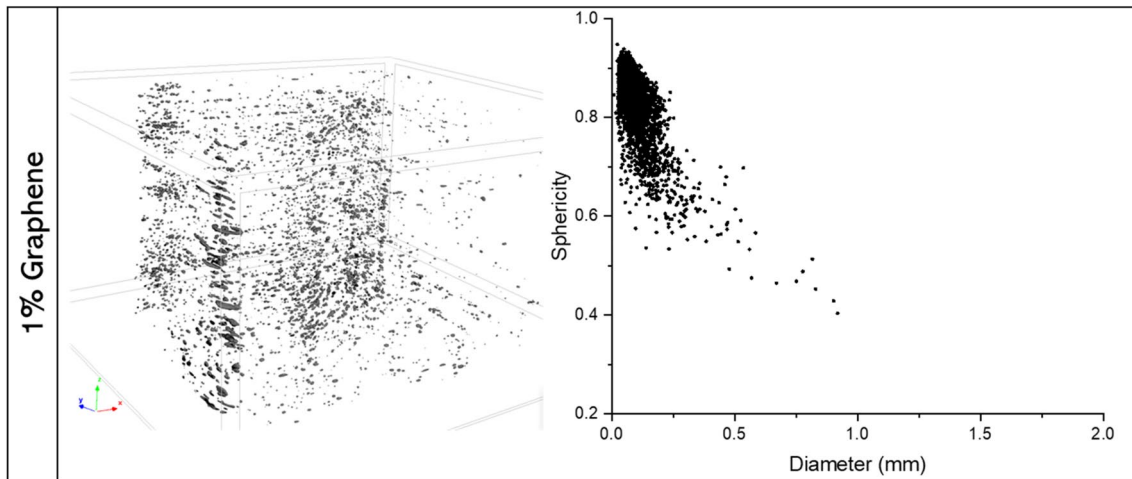


Fig. 18 Visual representation of distribution of 3D pores within 1% graphene–PEKK (left) and plot of major diameter vs sphericity of pores (right)

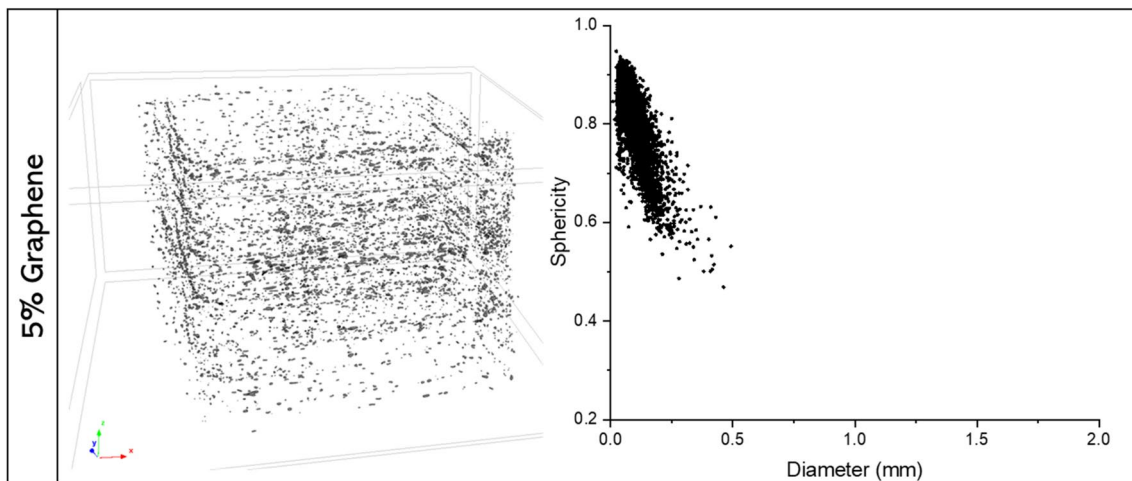


Fig. 19 Visual representation of distribution of 3D pores within 5% graphene–PEKK (left) and plot of major diameter vs sphericity of pores (right)

distribution of pores, followed by 1% graphene–PEKK and 1% GO–PEKK, respectively. Pores within neat PEKK and CNT–PEKK samples were more non-uniformly distributed in comparison. This indicates that graphene and GO may have enhanced the coalescence within layers and thus improved interlayer adhesion [123].

5.8 3D profilometry

3D profiles and corresponding average roughness (R_a) of top and side surfaces for neat PEKK, 1% graphene–PEKK, 5% graphene–PEKK, 1% GO–PEKK and CNT–PEKK are shown in Figs. 21, 22, 23, 24 and 25, respectively. The top surfaces of all specimens were smoother than the side surfaces, due to stair-stepping effect of side surfaces because

of layer-by-layer printing [124]. A clear distinction between layers can be observed in all samples except for 5% graphene–PEKK, which indicates an improved surface finish in 5% graphene–PEKK. This can be attributed to the higher crystallinity of the composite as observed from the DSC results (Sect. 5.2.2) in this study, which promotes layer shrinkage during printing and results in reduced voids between layers [125].

6 Conclusion

Graphene, graphene oxide and boron carbide particles were compatibilised with PEKK matrix using a twin-screw extruder to produce printable filaments for FFF.

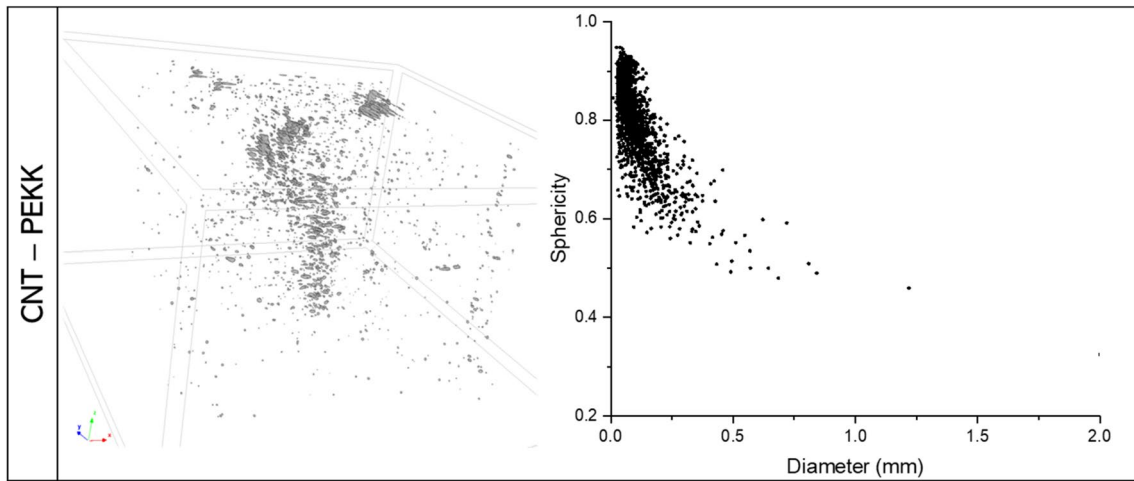


Fig. 20 Visual representation of pores within commercial CNT-reinforced PEKK (left) and plot of major diameter vs sphericity of pores (right)

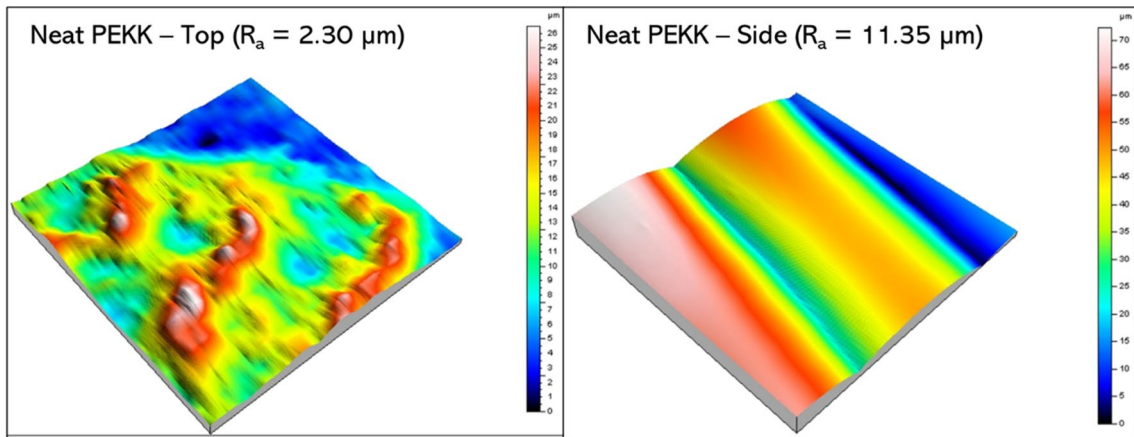


Fig. 21 3D profiles of top and side surface from neat PEKK sample

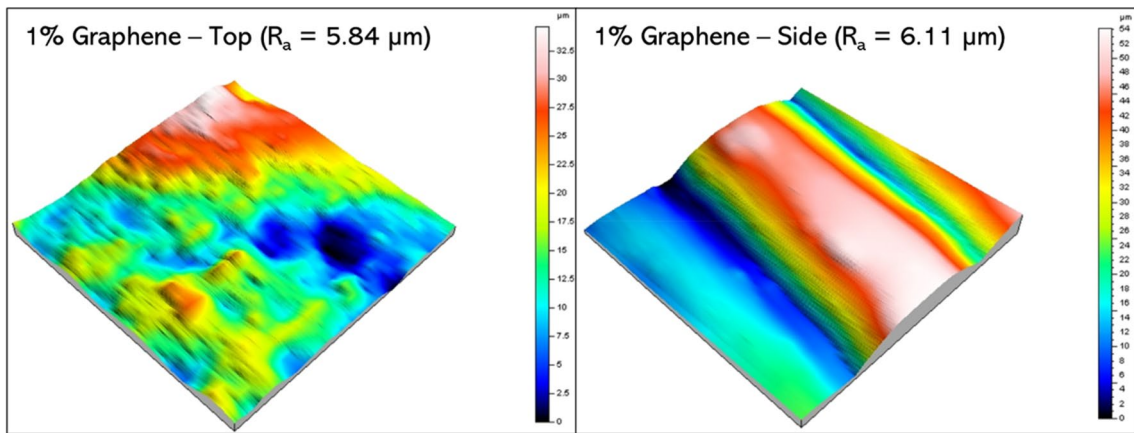


Fig. 22 3D profiles of top and side surface from 1% graphene-PEKK sample

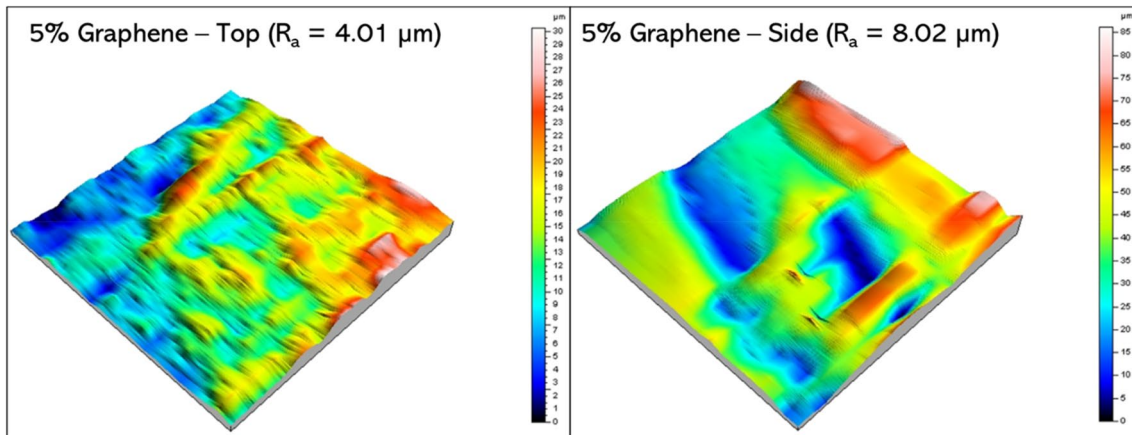


Fig. 23 3D profiles of top and side surface from 5% graphene–PEKK sample

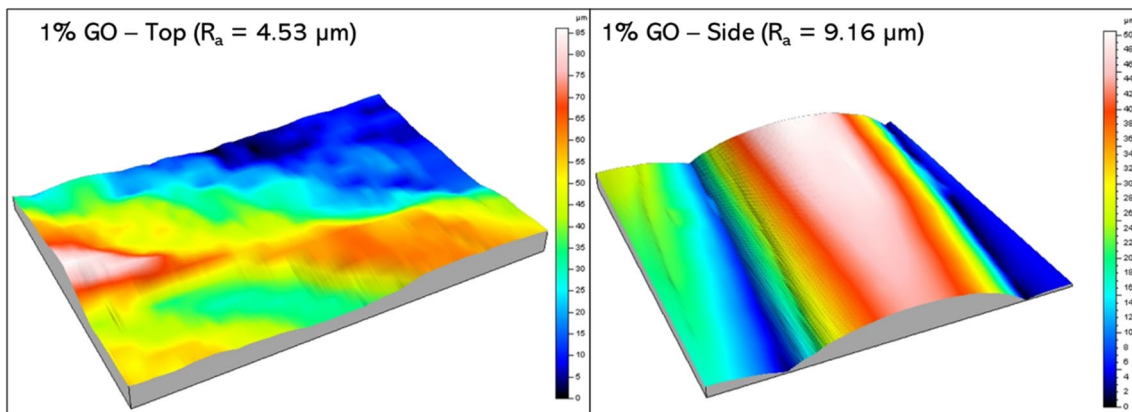


Fig. 24 3D profiles of top and side surface from 1% GO–PEKK sample

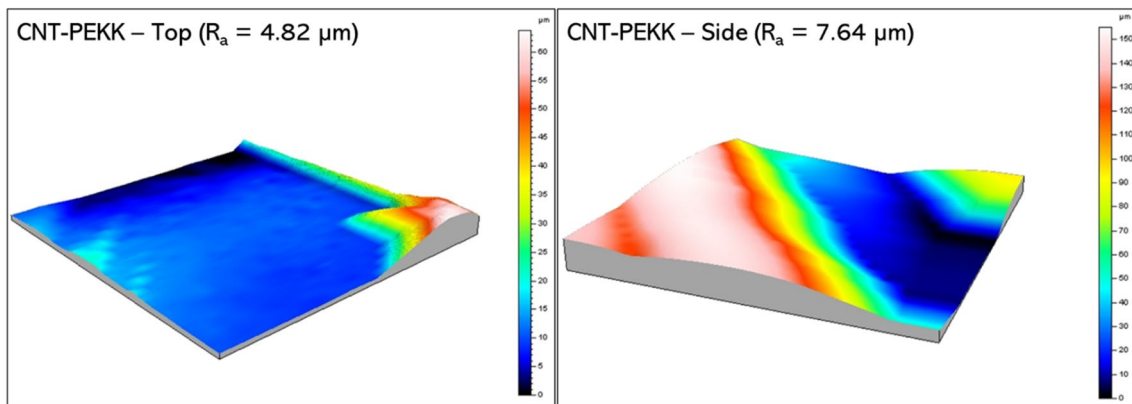


Fig. 25 3D profiles of top and side surface from commercial CNT–PEKK sample

Results from this study prove that graphene nano platelets produced the most printable filaments followed by graphene oxide. Boron carbide formed large agglomerates which affected printability. Char yield of neat PEKK

had increased due to all the additives, B_4C most significantly due to its high thermal stability as observed from TGA. DSC results showed that graphene and graphene oxide enhanced the non-isothermal melt crystallisation of

PEKK, but boron carbide did not influence crystallinity, possibly due to larger size of B₄C particles and formation of agglomerates which affected its ability to act as nucleating agent. A rheology study showed that all the additives increased the viscosity of neat PEKK except for graphene oxide which lubricated the polymer chains. However, the viscosity of all the developed composites was lower than commercial PEKK-based composites, and thus all formulations were considered printable.

Mechanical analysis of injection moulded composites showed that all additives improved the flexural modulus of PEKK, graphene most significantly followed by GO. The lower modulus of B₄C–PEKK in comparison can be attributed to the formation of agglomerates as observed in SEM images of cross-section. Morphology of filaments also showed signs of high percentage of intercalation in graphene–PEKK samples which was confirmed by XRD analysis. Hence, among the additives used, graphene was the most compatible filler material for PEKK matrix. Dimensions of the filaments suggested that only 1% graphene oxide, 1% and 5% graphene and neat PEKK were printable as other filaments were too thick due to properties such as viscosity and crystallinity. FT-IR spectra of PEKK and its composites confirmed that the chemical structure of PEKK was unaffected due to the additives. Parts were then printed using the printable filaments, and their porosity and 3D profilometry were studied. 1% GO–PEKK possessed the least percentage porosity which can be attributed to its low viscosity and thus higher flow. 3D profiles of side surfaces showed reduced void in 5% graphene-reinforced PEKK due to higher crystallinity of the composite as observed from DSC, which promotes layer shrinkage and thus reduced voids between layers. This study proves that with extrusion process modification and selection of appropriate particle size of additives, it is possible to manufacture multi-functional materials that can be printed using FFF process and has potential applications in space due to improved stiffness, char yield and electrical conductivity. Future studies should reinforce high-performance polymers with nano-sized boron carbide to obtain composite filaments with homogenous properties. Proton and neutron attenuation of the composites should also be studied using particle accelerators to determine if the additives can mitigate potential polymer degradation due to radiation in space.

Supplementary Information The online version contains supplementary material available at <https://doi.org/10.1007/s00170-024-13026-8>.

Acknowledgements The authors would like to acknowledge Jacinta White, Malisja de Vries and Heidi Cheng from the CSIRO Manufacturing Electron Microscopy and Surface Analysis Facility within the Characterisation Group for their contributions to this project. The authors also acknowledge the facilities and technical assistance of Advanced Manufacturing Precinct, Process Chemistry and Environmental Technical Services, Analytical Chemistry, and Australian Microscopy and

Microanalysis Facility, all of which are part of RMIT University Melbourne City Campus.

Author contribution All authors contributed to the study conception and design. 3D printing was performed by KR and AK. Filament extrusion and injection moulded samples were manufactured by MDO and KR. Data collection, analysis and preparation of the first draft were performed by KR. All authors commented on previous versions of the manuscript. All authors read and approved the final manuscript.

Funding Open Access funding enabled and organized by CAUL and its Member Institutions This study was funded by Australian Government Research Training Program Scholarship and The Commonwealth Scientific and Industrial Research Organisation (CSIRO).

Data availability The datasets generated during and/or analysed during the current study are available from the corresponding author on reasonable request.

Code availability Not applicable.

Declarations

Ethics approval Not applicable.

Consent to participate Not applicable.

Consent for publication Not applicable.

Conflict of interest The authors declare no competing interests.

Open Access This article is licensed under a Creative Commons Attribution 4.0 International License, which permits use, sharing, adaptation, distribution and reproduction in any medium or format, as long as you give appropriate credit to the original author(s) and the source, provide a link to the Creative Commons licence, and indicate if changes were made. The images or other third party material in this article are included in the article's Creative Commons licence, unless indicated otherwise in a credit line to the material. If material is not included in the article's Creative Commons licence and your intended use is not permitted by statutory regulation or exceeds the permitted use, you will need to obtain permission directly from the copyright holder. To view a copy of this licence, visit <http://creativecommons.org/licenses/by/4.0/>.

References

1. Auletti CR, Martino AJ, Sheinman OR (2016) A mission of firsts. NASA cutting edge, vol 12(2) Available at: <https://www.nasa.gov/goddard/technology/cuttingedge-archive/>. Accessed 17 Jan 2024
2. Standardization ECfS (2008) ECSS-Q-ST-70-02C Space product assurance: thermal vacuum outgassing test for the screening of space materials. European Cooperation for Space Standardization. Available at: <https://ecss.nl/standard/ecss-q-st-70-02c-thermal-vacuum-outgassing-test-for-the-screening-of-space-materials/>
3. Leach RD, Alexander MB (1995) Failures and anomalies attributed to spacecraft charging. NASA Reference Publication 1375. Available at: <https://ntrs.nasa.gov/citations/19960001539>
4. Standardization ECfS (2019) ECSS-Q-ST-70C Rev.2 Space product assurance: materials, mechanical parts and processes. ECSS Secretariat Requirements & Standards Division. Noordwijk, The Netherlands. Available at: <https://ecss.nl/standard/>

- [ecss-q-st-70c-rev-2-materials-mechanical-parts-and-processes-15-october-2019/](#)
- Thornton EA (1996) Thermal structures for aerospace applications. AIAA Education Series. American Institute of Aeronautics and Astronautics, Inc., USA
 - Ghidini T (2018) Materials for space exploration and settlement. *Nat Mater* 17(10):846. <https://doi.org/10.1038/s41563-018-0184-4>
 - Han J-H, Kim C-G (2006) Low earth orbit space environment simulation and its effects on graphite/epoxy composites. *Compos Struct* 72(2):218–226. <https://doi.org/10.1016/j.compstruct.2004.11.007>
 - Rival G, Paulmier T, Dantras E (2019) Influence of electronic irradiations on the chemical and structural properties of PEEK for space applications. *Polym Degrad Stab* 168:108943
 - Hu LY, Yang S, Miller AK, Park CS, Plichta KA, Rochford SJ, Schulz ME, Orwoll RA, Jensen BJ (2006) Aliphatic/aromatic hybrid polymers for functionally graded radiation shielding. *High Perform Polym* 18(2):213–225. <https://doi.org/10.1177/0954008306059342>
 - Leary M, Mazur M, Watson M, Boileau E, Brandt M (2019) Voxel-based support structures for additive manufacture of topologically optimal geometries. *Int J Adv Manuf Technol* 105(1):1–26. <https://doi.org/10.1007/s00170-019-03964-z>
 - Cowley A, Perrin J, Meurisse A, Micallef A, Fateri M, Rinaldo L, Bamsey N, Sperl M (2019) Effects of variable gravity conditions on additive manufacture by fused filament fabrication using polylactic acid thermoplastic filament. *Addit Manuf* 28:814–820. <https://doi.org/10.1016/j.addma.2019.06.018>
 - Ledbetter FE, III, Prater TJ, Ryan RM, Bean QA, Rolin TD, Werkheiser NJ, Beshears RD, Ordonez EA (2016) Summary report on phase I results from the 3D printing in zero G technology demonstration mission. Vol I. NASA. <https://ntrs.nasa.gov/api/citations/20160008972/downloads/20160008972.pdf>. Accessed 18 Aug 2023
 - Musso G, Lentini G, Enrietti L, Volpe C, Ambrosio EP, Lorusso M, Mascetti G, Valentini G, Goonetilleke R, Karwowski W (2016) Portable on orbit printer 3D: 1st European additive manufacturing machine on International Space Station. *Adv Phys Ergon Hum Factors* 489:1564–1655. https://doi.org/10.1007/978-3-319-41694-6_62
 - Elhajjar R, Gill T (2016) Chapter 5: design of a carbon-fiber reinforced fused deposition modeling modular wrench tool. In: *Studies into additive manufacturing for in-space manufacturing: student research papers*. SAE, pp 37–52. <https://ieeexplore.ieee.org/document/8504750>
 - Zanjanijam AR, Major I, Lyons JG, Lafont U, Devine DM (2020) Fused filament fabrication of PEEK: a review of process-structure-property relationships. *Polymers* 12(8):1665. <https://doi.org/10.3390/polym12081665>
 - Gibson I, Rosen D, Stucker B (2015) *Additive manufacturing technologies 3D printing, rapid prototyping, and direct digital manufacturing*. 2nd ed. Springer, New York
 - Becedas J, Caparros A, Morillo P, Flores GR, Urteaga JM (2018) Redesign & space qualification of a 3D-printed satellite structure: with polyetherimide. *J Br Interplanet Soc* 71(11):416–425
 - Kalra S, Munjal BS, Singh VR, Mahajan M, Bhattacharya B (2019) Investigations on the suitability of PEEK material under space environment conditions and its application in a parabolic space antenna. *Adv Space Res* 63(12):4039–4045. <https://doi.org/10.1016/j.asr.2019.03.006>
 - Yap T, Heathman N, Phillips T, Beaman J, Tehrani M (2023) Additive manufacturing of polyaryletherketone (PAEK) polymers and their composites. *Compos B: Eng* 266:111019. <https://doi.org/10.1016/j.compositesb.2023.111019>
 - Reber Iii R, Koo B, Liu D (2019) Polyetherketoneketone (PEKK), a versatile ultra-polymer for additive manufacturing. Paper presented at the SAMPE 2019 - Charlotte, NC. <https://doi.org/10.33599/nasampe/s.19.1596>
 - Leigh SJ, Bradley RJ, Purssell CP, Billson DR, Hutchins DA (2012) A simple, low-cost conductive composite material for 3D printing of electronic sensors. *PLoS one* 7(11):e49365
 - Postiglione G, Natale G, Griffini G, Levi M, Turri S (2015) Conductive 3D microstructures by direct 3D printing of polymer/carbon nanotube nanocomposites via liquid deposition modeling. *Compos A: Appl Sci Manuf* 76:110–114. <https://doi.org/10.1016/j.compositesa.2015.05.014>
 - Gnanasekaran K, Heijmans T, van Bennekom S, Woldhuis H, Wijnia S, de With G, Friedrich H (2017) 3D printing of CNT- and graphene-based conductive polymer nanocomposites by fused deposition modeling. *Appl Mater Today* 9:21–28. <https://doi.org/10.1016/j.apmt.2017.04.003>
 - Otten RHJ, van der Schoot P (2009) Continuum percolation of polydisperse nanofillers. *Phys Rev Lett* 103(22):225704. <https://doi.org/10.1103/PhysRevLett.103.225704>
 - Gnanasekaran K, de With G, Friedrich H (2014) On packing, connectivity, and conductivity in mesoscale networks of polydisperse multiwalled carbon nanotubes. *J Phys Chem C* 118(51):29796–29803. <https://doi.org/10.1021/jp5081669>
 - Gnanasekaran K, de With G, Friedrich H (2016) Quantitative analysis of connectivity and conductivity in mesoscale multiwalled carbon nanotube networks in polymer composites. *J Phys Chem C* 120(48):27618–27627. <https://doi.org/10.1021/acs.jpcc.6b07458>
 - Kishore V, Ajinjeru C, Duty CE, Hassen AA, Lindahl JM, Liu P, Kunc V (2017) Rheological characteristics of fiber reinforced poly(ether ketone ketone)(PEKK) for melt extrusion additive manufacturing. Paper presented at the SAMPE 2017. Seattle, USA. <https://www.osti.gov/biblio/1474726>
 - Choupin T, Fayolle B, Régnier G, Paris C, Cinquin J, Brulé B (2017) Isothermal crystallization kinetic modeling of poly(etherketoneketone) (PEKK) copolymer. *Polymer* 111:73
 - Choupin T, Fayolle B, Régnier G, Paris C, Cinquin J, Brulé B (2018) A more reliable DSC-based methodology to study crystallization kinetics: application to poly(ether ketone ketone) (PEKK) copolymers. *Polymer* 155:109–115. <https://doi.org/10.1016/j.polymer.2018.08.060>
 - Labouriau A, Robison T, Shonrock C, Simmonds S, Cox B, Pacheco A, Cady C (2018) Boron filled siloxane polymers for radiation shielding. *Radiat Phys Chem* 144:288–294. <https://doi.org/10.1016/j.radphyschem.2017.08.027>
 - Stephens JM, Glasgow MB, Kiefer RL, Orwoll RA, Long SAT (1992) Radiation effects on films of boron-loaded polymers. *Polym Prepr (Am Chem Soc, Div Polym Chem)* 33(1):1152
 - Shin JW, Lee J-W, Yu S, Baek BK, Hong JP, Seo Y, Kim WN, Hong SM, Koo CM (2014) Polyethylene/boron-containing composites for radiation shielding. *Thermochim Acta* 585:5–9. <https://doi.org/10.1016/j.tca.2014.03.039>
 - Woosley S, Abuali Galehdari N, Kelkar A, Aravamudan S (2018) Fused deposition modeling 3D printing of boron nitride composites for neutron radiation shielding. *J Mater Res* 33(22):3657–3664. <https://doi.org/10.1557/jmr.2018.316>
 - Suri AK, Subramanian C, Sonber JK, Murthy TSRC (2010) Synthesis and consolidation of boron carbide: a review. *Int Mater Rev* 55(1):4–40. <https://doi.org/10.1179/095066009X12506721665211>
 - Diaz-Cano A, Trice RW, Youngblood JP (2017) Stabilization of highly-loaded boron carbide aqueous suspensions. *Ceram Int* 43(12):8572–8578. <https://doi.org/10.1016/j.ceramint.2017.03.111>

36. Wu Y, Cao Y, Wu Y, Li D (2020) Neutron shielding performance of 3D-printed boron carbide PEEK composites. *Materials* 13(10):2314. <https://doi.org/10.3390/ma13102314>
37. Renteria JD, Nika DL, Balandin AA (2014) Graphene thermal properties: applications in thermal management and energy storage. *Appl Sci* 4(4):525–547. <https://doi.org/10.3390/app4040525>
38. Balandin AA (2011) Thermal properties of graphene and nanostructured carbon materials. *Nat Mater* 10(8):569–581
39. Yan Z, Liu G, Khan JM, Balandin AA (2012) Graphene quilts for thermal management of high-power GaN transistors. *Nat Commun* 3(1):1–8
40. Goyal V, Balandin AA (2012) Thermal properties of the hybrid graphene-metal nano-micro-composites: applications in thermal interface materials. *Appl Phys Lett* 100(7):073113
41. Goli P, Legedza S, Dhar A, Salgado R, Renteria J, Balandin AA (2014) Graphene-enhanced hybrid phase change materials for thermal management of Li-ion batteries. *J Power Sources* 248:37–43
42. Shahil KM, Balandin AA (2012) Thermal properties of graphene and multilayer graphene: applications in thermal interface materials. *Solid State Commun* 152(15):1331–1340
43. Hassan K, Nine MJ, Tung TT, Stanley NJ, Yap PL, Rastin H, Yu L, Losic D (2020) Functional inks and extrusion-based 3D printing of 2D materials: a review of current research and applications. *Nanoscale*. <https://doi.org/10.1039/D0NR04933F>
44. Dul S, Fambri L, Pegoretti A (2016) Fused deposition modeling with ABS-graphene nanocomposites. *Compos A: Appl Sci Manuf* 85:181–191. <https://doi.org/10.1016/j.compositesa.2016.03.013>
45. Tambrallimath V, Keshavamurthy R, D S, Koppad PG, Kumar GSP (2019) Thermal behavior of PC-ABS based graphene filled polymer nanocomposite synthesized by FDM process. *Compos Commun* 15:129–134. <https://doi.org/10.1016/j.coco.2019.07.009>
46. Zhu D, Ren Y, Liao G, Jiang S, Liu F, Guo J, Xu G (2017) Thermal and mechanical properties of polyamide 12/graphene nanoplatelets nanocomposites and parts fabricated by fused deposition modeling. *J Appl Polym Sci* 134(39):45332. <https://doi.org/10.1002/app.45332>
47. Bustillos J, Montero D, Nautiyal P, Loganathan A, Boesl B, Agarwal A (2018) Integration of graphene in poly(lactic) acid by 3D printing to develop creep and wear-resistant hierarchical nanocomposites. *Polym Compos* 39(11):3877–3888. <https://doi.org/10.1002/polb.24422>
48. Caminero MÁ, Chacón JM, García-Plaza E, Núñez PJ, Reverte JM, Becar JP (2019) Additive manufacturing of PLA-based composites using fused filament fabrication: effect of graphene nanoplatelet reinforcement on mechanical properties, dimensional accuracy and texture. *Polymers* 11(5):799. <https://doi.org/10.3390/polym11050799>
49. Arif MF, Alhashmi H, Varadarajan KM, Koo JH, Hart AJ, Kumar S (2020) Multifunctional performance of carbon nanotubes and graphene nanoplatelets reinforced PEEK composites enabled via FFF additive manufacturing. *Composites* 184:107625. <https://doi.org/10.1016/j.compositesb.2019.107625>
50. Bessaguet C, Dantras E, Michon G, Chevalier M, Laffont L, Lacabanne C (2019) Electrical behavior of a graphene/PEKK and carbon black/PEKK nanocomposites in the vicinity of the percolation threshold. *J Non-Cryst Solids* 512:1–6. <https://doi.org/10.1016/j.jnoncrysol.2019.02.017>
51. Dideikin AT, Vul AY (2019) Graphene oxide and derivatives: the place in graphene family. *Front Phys* 6:2296–424X. <https://doi.org/10.3389/fphy.2018.00149>
52. Li F, Hua Y, Qu C-B, Xiao H-M, Fu S-Y (2016) Greatly enhanced cryogenic mechanical properties of short carbon fiber/polyethersulfone composites by graphene oxide coating. *Compos A* 89:47–55. <https://doi.org/10.1016/j.compositesa.2016.02.016>
53. Laurenzi S, de Zanet G, Santonicola MG (2020) Numerical investigation of radiation shielding properties of polyethylene-based nanocomposite materials in different space environments. *Acta Astronaut* 170:530–538. <https://doi.org/10.1016/j.actaastro.2020.02.027>
54. Jackson P, Jacobsen NR, Baun A, Birkedal R, Kühnel D, Jensen KA, Vogel U, Wallin H (2013) Bioaccumulation and ecotoxicity of carbon nanotubes. *Chem Cent J* 7(1):154. <https://doi.org/10.1186/1752-153X-7-154>
55. Martín N, Guldi DM (2010) Carbon nanotubes and related structures: synthesis, characterization, functionalization, and applications. John Wiley & Sons
56. Volder MFLD, Tawfick SH, Baughman RH, Hart AJ (2013) Carbon Nanotubes: Present and Future Commercial Applications. *Science* 339(6119):535–539. <https://doi.org/10.1126/science.1222453>
57. ULTEM™ RESIN (2023) SABIC. <https://www.sabic.com/en/products/specialties/ultem-resin-family-of-high-heat-solutions/ultem-resin>. Accessed 1 Dec 2023
58. Gardner JM, Sauti G, Kim J-W, Cano RJ, Wincheski RA, Stelter CJ, Grimsley BW, Working DC, Siochi EJ (2016) 3-D printing of multifunctional carbon nanotube yarn reinforced components. *Addit Manuf* 12:38–44. <https://doi.org/10.1016/j.addma.2016.06.008>
59. Rigotti D, Fambri L, Pegoretti A (2018) Polyvinyl alcohol reinforced with carbon nanotubes for fused deposition modeling. *J Reinf Plast Compos* 37(10):716–727. <https://doi.org/10.1177/0731684418761224>
60. Berretta S, Davies R, Shyng YT, Wang Y, Ghita O (2017) Fused Deposition Modelling of high temperature polymers: exploring CNT PEEK composites. *Polym Testing* 63:251–262. <https://doi.org/10.1016/j.polymertesting.2017.08.024>
61. Ning F, Cong W, Qiu J, Wei J, Wang S (2015) Additive manufacturing of carbon fiber reinforced thermoplastic composites using fused deposition modeling. *Compos B: Eng* 80:369–378. <https://doi.org/10.1016/j.compositesb.2015.06.013>
62. Stepashkin AA, Chukov DI, Senatov FS, Salimon AI, Korsunsky AM, Kaloshkin SD (2018) 3D-printed PEEK-carbon fiber (CF) composites: structure and thermal properties. *Compos Sci Technol* 164:319–326. <https://doi.org/10.1016/j.compscitech.2018.05.032>
63. Prüß H, Vietor T (2015) Design for fiber-reinforced additive manufacturing. *J Mech Des* 137(11). <https://doi.org/10.1115/1.4030993>
64. Ghimire R, Liou F (2021) Experimental investigation of additive manufacturing of continuous carbon fiber composites with multifunctional electro-tensile properties. *Materials* 14(21):6574-undefined. <https://doi.org/10.3390/ma14216574>
65. Pandelidi C, Bateman S, Maghe M, Piegert S, Brandt M (2022) Fabrication of continuous carbon fibre-reinforced polyetherimide through fused filament fabrication. *Prog Addit Manuf*. <https://doi.org/10.1007/s40964-022-00284-9>
66. Li Q, Zhao W, Li Y, Yang W, Wang G (2019) Flexural properties and fracture behavior of CF/PEEK in orthogonal building orientation by FDM: microstructure and mechanism. *Polymers* 11(4):656. <https://doi.org/10.3390/polym11040656>
67. Prashantha K, Roger F (2017) Multifunctional properties of 3D printed poly(lactic acid)/graphene nanocomposites by fused deposition modeling. *J Macromol Sci A Pure Appl Chem* 54(1):24–29. <https://doi.org/10.1080/10601325.2017.1250311>
68. Lowe SE, Shi G, Zhang Y, Qin J, Wang S, Uijtendaal A, Sun J, Jiang L, Jiang S, Qi D, Al-Mamun M, Liu P, Zhong YL, Zhao H (2019) Scalable production of graphene oxide using a 3D-printed packed-bed electrochemical reactor with a boron-doped diamond

- electrode. *ACS Appl Nano Mater* 2(2):867–878. <https://doi.org/10.1021/acsnm.8b02126>
69. Liu L, Xiao L, Zhang X, Li M, Chang Y, Shang L, Ao Y (2015) Improvement of the thermal conductivity and friction performance of poly (ether ether ketone)/carbon fiber laminates by addition of graphene. *RSC Adv* 5(71):57853–57859
 70. Aumnate C, Potiyaraj P, Saengow C, Giacomini AJ (2021) Reinforcing polypropylene with graphene-poly(lactic acid) microcapsules for fused-filament fabrication. *Mater Des* 198:109329. <https://doi.org/10.1016/j.matdes.2020.109329>
 71. Schellhase KJ, Koo JH, Buffy J, Brushaber R (2017) Development of new thermal protection systems based on silica/poly-siloxane composites. In: 58th AIAA/ASCE/AHS/ASC Struct Struct Dyn Mater Conf. <https://doi.org/10.2514/6.2017-1367>
 72. Quiroga Cortés L, Caussé N, Dantras E, Lonjon A, Lacabanne C (2016) Morphology and dynamical mechanical properties of poly ether ketone ketone (PEKK) with meta phenyl links. *J Appl Polym Sci* 133(19):43396. <https://doi.org/10.1002/app.43396>
 73. Ajinjeru C, Kishore V, Lindahl J, Sudbury Z, Hassen A, Post B, Love L, Kunc V, Duty C (2018) The influence of dynamic rheological properties on carbon fiber-reinforced polyetherimide for large-scale extrusion-based additive manufacturing. *Int J Adv Manuf Technol* 99(1–4):411–418. <https://doi.org/10.1007/s00170-018-2510-z>
 74. Ajinjeru C, Kishore V, Chen X, Lindahl J, Sudbury Z, Hassen AA, Kunc V, Post B, Love L, Duty C (2016) The influence of rheology on melt processing conditions of amorphous thermoplastics for big area additive manufacturing (BAAM). Paper presented at the 27th Annual Solid Freeform Fabrication Symposium. pp 754–761. <https://repositories.lib.utexas.edu/items/8953fd22-207f-4b65-b316-d637c9ff5322>
 75. Richardsson MJ, Wu H, Wilcox TJ, Broaddus M, Lin PC, Krifa M, Koo JH (2017) Flame retardant nylon 6 nanocomposites for fused deposition modeling (FDM) applications. Paper presented at the International SAMPE Technical Conference 2017. Seattle, USA
 76. Wu H, Sulkis M, Driver J, Saade-Castillo A, Thompson A, Koo JH (2018) Multi-functional ULTEM™1010 composite filaments for additive manufacturing using Fused Filament Fabrication (FFF). *Addit Manuf* 24:298–306. <https://doi.org/10.1016/j.addma.2018.10.014>
 77. ASTM (2017) ASTM D790–03 Standard test methods for flexural properties of unreinforced and reinforced plastics and electrical insulating materials. ASTM International. <https://doi.org/10.1520/D0790-03>
 78. Rashed K, Kafi A, Simons R, Bateman S (2023) Optimization of material extrusion additive manufacturing process parameters for polyether ketone ketone (PEKK). *Int J Adv Manuf Technol* 126(3):1067–1091. <https://doi.org/10.1007/s00170-023-11167-w>
 79. Taherian R (2014) Development of an equation to model electrical conductivity of polymer-based carbon nanocomposites. *ECS J Solid State Sci Technol* 3(6):M26. <https://doi.org/10.1149/2.023406jss>
 80. Fontaine P, Weiss-Hortala E, Botaro V, Paiva JMF, Soudais Y (2021) Impact of atmosphere on recovered carbon fibers from poly ether ether ketone (PEEK) Based composites during thermoconversion. *Waste Biomass Valor* 12(12):6389–6402. <https://doi.org/10.1007/s12649-021-01445-7>
 81. Levchik SV, Weil ED, Lewin M (1999) Thermal decomposition of aliphatic nylons. *Polym Int* 48(7):532–557. [https://doi.org/10.1002/\(SICI\)1097-0126\(199907\)48:7<3c532::AID-PI214%3e3.0.CO;2-R](https://doi.org/10.1002/(SICI)1097-0126(199907)48:7<3c532::AID-PI214%3e3.0.CO;2-R)
 82. Sulkis MC, Driver J, Saade-Castillo A, Thompson A, Wu H, Koo JH (2018) Additive manufacturing of thermal protection system materials. Paper presented at the 2018 AIAA/ASCE/AHS/ASC Structures, structural dynamics, and materials conference. Florida, USA. <https://doi.org/10.2514/6.2018-0092>
 83. Wu H, Ortiz R, Correa RDA, Krifa M, Koo JH (2018) Self-extinguishing and non-drip flame retardant polyamide 6 nanocomposite: mechanical, thermal, and combustion behavior. *Flame Retardancy Therm Stab Mater* 1(1):1–13. <https://doi.org/10.1515/fret-2018-0001>
 84. Yuan B, Fan A, Yang M, Chen X, Hu Y, Bao C, Jiang S, Niu Y, Zhang Y, He S, Dai H (2017) The effects of graphene on the flammability and fire behavior of intumescent flame retardant polypropylene composites at different flame scenarios. *Polym Degrad Stab* 143:42–56. <https://doi.org/10.1016/j.polyimdegrastab.2017.06.015>
 85. Cao C-F, Yu B, Chen Z-Y, Qu Y-X, Li Y-T, Shi Y-Q, Ma Z-W, Sun F-N, Pan Q-H, Tang L-C, Song P, Wang H (2022) Fire intumescent, high-temperature resistant, mechanically flexible graphene oxide network for exceptional fire shielding and ultra-fast fire warning. *Nano-Micro Lett* 14(1):92. <https://doi.org/10.1007/s40820-022-00837-1>
 86. Rallini M, Natali M, Kenny JM, Torre L (2013) Effect of boron carbide nanoparticles on the fire reaction and fire resistance of carbon fiber/epoxy composites. *Polymer* 54(19):5154–5165. <https://doi.org/10.1016/j.polymer.2013.07.038>
 87. Akinyi C, Longun J, Chen S, Iroh JO (2021) Decomposition and flammability of polyimide graphene composites. *Minerals* 11(2):168. <https://doi.org/10.3390/min11020168>
 88. Rallini M, Torre L, Kenny J, Natali M (2017) Effect of boron carbide nanoparticles on the thermal stability of carbon/phenolic composites. *Polym Compos* 38(9):1819–1827. <https://doi.org/10.1002/pc.23752>
 89. Solati M, Saeidi A, Ghasemi I (2019) The effect of graphene nanoplatelets on dynamic properties, crystallization, and morphology of a biodegradable blend of poly(lactic acid)/thermoplastic starch. *Iran Polym J* 28(8):649–658. <https://doi.org/10.1007/s13726-019-00731-5>
 90. Razeghi M, Pircheraghi G (2018) TPU/graphene nanocomposites: effect of graphene functionality on the morphology of separated hard domains in thermoplastic polyurethane. *Polymer* 148:169–180. <https://doi.org/10.1016/j.polymer.2018.06.026>
 91. Pedoto G, Grandidier J-C, Gigliotti M, Vinet A (2022) Characterization and modelling of the PEKK thermomechanical and creep behavior above the glass transition temperature. *Mech Mater* 166:104189. <https://doi.org/10.1016/j.mechmat.2021.104189>
 92. Wang H, Qiu Z (2012) Crystallization kinetics and morphology of biodegradable poly(L-lactic acid)/graphene oxide nanocomposites: influences of graphene oxide loading and crystallization temperature. *Thermochim Acta* 527:40–46. <https://doi.org/10.1016/j.tca.2011.10.004>
 93. Shenoy AV (1999) Unsteady shear viscoelastic properties. In: *Rheology of filled polymer systems*. Springer, Dordrecht. pp 338–394. https://doi.org/10.1007/978-94-015-9213-0_8
 94. Arrigo R, Frache A (2022) FDM Printability of PLA based-materials: the key role of the rheological behavior. *Polymers* 14(9):1754. <https://doi.org/10.3390/polym14091754>
 95. Duty C, Ajinjeru C, Kishore V, Compton B, Hmeidat N, Chen X, Liu P, Hassen AA, Lindahl J, Kunc V (2018) What makes a material printable? A viscoelastic model for extrusion-based 3D printing of polymers. *J Manuf Process* 35(C):526–537. <https://doi.org/10.1016/j.jmappro.2018.08.008>
 96. Mohanty RM, Balasubramanian K, Seshadri SK (2008) Boron carbide-reinforced aluminum 1100 matrix composites: fabrication and properties. *Mater Sci Eng A* A498(1–2):42–52. <https://doi.org/10.1016/j.msea.2007.11.154>
 97. Di Carlo S, De Angelis F, Brauner E, Pranno N, Tassi G, Senatore M, Bossù M (2020) Flexural strength and elastic modulus

- evaluation of structures made by conventional PMMA and PMMA reinforced with graphene. *Eur Rev Med Pharmacol Sci* 24(10):5201–5208. https://doi.org/10.26355/eurrev_202005_21301
98. Du S-S, Li F, Xiao H-M, Li Y-Q, Hu N, Fu S-Y (2016) Tensile and flexural properties of graphene oxide coated-short glass fiber reinforced polyethersulfone composites. *Compos B* 99:407–415. <https://doi.org/10.1016/j.compositesb.2016.06.023>
 99. Fang L, Yan Y, Agarwal O, Yao S, Seppala JE, Kang SH (2020) Effects of environmental temperature and humidity on the geometry and strength of polycarbonate specimens prepared by fused filament fabrication. *Materials* 13(19):4414. <https://doi.org/10.3390/ma13194414>
 100. Simunec DP, Jacob J, Kandjani AEZ, Trinchi A, Sola A (2023) Facilitating the additive manufacture of high-performance polymers through polymer blending: a review. *Eur Polymer J* 201:112553. <https://doi.org/10.1016/j.eurpolymj.2023.112553>
 101. Cadwell CE (1997) Vacuum sizing apparatus and method of using same. Google Patents US5607638A. <https://patents.google.com/patent/US5607638A/en>
 102. Ahmad I, Jabeen N, Ahmad W (2022) Fabrication and characterization of boron carbide/polymethyl methacrylate composites. *Fullerenes Nanotubes Carbon Nanostruct* 30(7):727–734. <https://doi.org/10.1080/1536383X.2021.2016709>
 103. Shen Q, Wu C, Luo G, Fang P, Li C, Wang Y, Zhang L (2014) Microstructure and mechanical properties of Al-7075/B4C composites fabricated by plasma activated sintering. *J Alloy Compd* 588:265–270. <https://doi.org/10.1016/j.jallcom.2013.11.089>
 104. Chisena RS, Engstrom SM, Shih AJ (2020) Computed tomography evaluation of the porosity and fiber orientation in a short carbon fiber material extrusion filament and part. *Addit Manuf* 34:101189. <https://doi.org/10.1016/j.addma.2020.101189>
 105. Wang J, He Y, Xie Z, Chen C, Yang Q, Zhang C, Wang B, Zhan Y, Zhao T (2018) Functionalized boron carbide for enhancement of anticorrosion performance of epoxy resin. *Polym Adv Technol* 29(2):758–766. <https://doi.org/10.1002/pat.4181>
 106. Uhm YR, Kim J, Jung J, Rhee CK (2009) Fabrications of PVA coated nano-B4C reinforced HDPE composites. *Mod Phys Lett B* 23(31 & 32):3931–3936
 107. Li X, Wu J, Tang C, He Z, Yuan P, Sun Y, Lau W-m, Zhang K, Mei J, Huang Y (2019) High temperature resistant polyimide/boron carbide composites for neutron radiation shielding. *Compos B* 159:355–361. <https://doi.org/10.1016/j.compositesb.2018.10.003>
 108. Yudin VE, Svetlichnyi VM, Shumakov AN, Schechter R, Harel H, Marom G (2008) Morphology and mechanical properties of carbon fiber reinforced composites based on semicrystalline polyimides modified by carbon nanofibers. *Compos A: Appl Sci Manuf* 39(1):85–90. <https://doi.org/10.1016/j.compositesa.2007.08.026>
 109. Chen J, Long Z, Wang S, Meng Y, Zhang G, Nie S (2019) Biodegradable blends of graphene quantum dots and thermoplastic starch with solid-state photoluminescent and conductive properties. *Int J Biol Macromol* 139:367–376. <https://doi.org/10.1016/j.ijbiomac.2019.07.211>
 110. Bher A, Uysal Unalan I, Auras R, Rubino M, Schvezov CE (2018) Toughening of poly(lactic acid) and thermoplastic cassava starch reactive blends using graphene nanoplatelets. *Polymers* 10(1):95. <https://doi.org/10.3390/polym10010095>
 111. Whitaker JD, Caldwell RJ, Jennings C (2016) Methods of preparing articles by electrodeposition and additive manufacturing processes. WO/2016/044712. <https://patentscope.wipo.int/search/en/detail.jsf?docId=WO2016044712>
 112. Baek I, Lim C-M, Park KY, Ryu BK (2022) Enhanced metal coating adhesion by surface modification of 3D printed PEKKs. *Coatings* 12(6):854. <https://doi.org/10.3390/coatings12060854>
 113. Tan JC, Low HY (2018) Embedded electrical tracks in 3D printed objects by fused filament fabrication of highly conductive composites. *Addit Manuf* 23:294–302. <https://doi.org/10.1016/j.addma.2018.06.009>
 114. Dorigato A, Moretti V, Dul S, Unterberger SH, Pegoretti A (2017) Electrically conductive nanocomposites for fused deposition modelling. *Synth Met* 226:7–14. <https://doi.org/10.1016/j.synthmet.2017.01.009>
 115. Spinelli G, Kotsilkova R, Ivanov E, Petrova-Doycheva I, Menseidov D, Georgiev V, Di Maio R, Silvestre C (2020) Effects of filament extrusion, 3D printing and hot-pressing on electrical and tensile properties of poly(lactic) acid composites filled with carbon nanotubes and graphene. *Nanomaterials* 10(1):35. <https://doi.org/10.3390/nano10010035>
 116. Özen A, Abali BE, Völlmecke C, Gerstel J, Auhl D (2021) Exploring the role of manufacturing parameters on microstructure and mechanical properties in fused deposition modeling (FDM) using PETG. *Appl Compos Mater* 28(6):1799–1828. <https://doi.org/10.1007/s10443-021-09940-9>
 117. Al-Hasni S, Santori G (2020) 3D printing of vacuum and pressure tight polymer vessels for thermally driven chillers and heat pumps. *Vacuum* 171:109017. <https://doi.org/10.1016/j.vacuum.2019.109017>
 118. Pandelidi C, Maconachie T, Bateman S, Kelbassa I, Piegert S, Leary M, Brandt M (2021) Parametric study on tensile and flexural properties of ULTEM 1010 specimens fabricated via FDM. *Rapid Prototyp J* 27(2):429–451. <https://doi.org/10.1108/RPJ-10-2019-0274>
 119. Pandelidi C, Lee KPM, Kajtaz M (2021) Effects of polyamide-11 powder refresh ratios in multi-jet fusion: a comparison of new and used powder. *Addit Manuf* 40:101933. <https://doi.org/10.1016/j.addma.2021.101933>
 120. Dewulf W, Pavan M, Craeghs T, Kruth J-P (2016) Using X-ray computed tomography to improve the porosity level of polyamide-12 laser sintered parts. *CIRP Ann* 65(1):205–208. <https://doi.org/10.1016/j.cirp.2016.04.056>
 121. Bagheri G, Bonadonna C (2016) Chapter 2 - aerodynamics of volcanic particles: characterization of size, shape, and settling velocity. In: Mackie S, Cashman K, Ricketts H, Rust A, Watson M (eds) *Volcanic Ash*. Elsevier, Geneva. pp 39–52. <https://doi.org/10.1016/B978-0-08-100405-0.00005-7>
 122. Jiang L, Chawla N, Pacheco M, Noveski V (2011) Three-dimensional (3D) microstructural characterization and quantification of reflow porosity in Sn-rich alloy/copper joints by X-ray tomography. *Mater Charact* 62(10):970–975. <https://doi.org/10.1016/j.matchar.2011.07.011>
 123. Lepoivre A, Levy A, Boyard N, Gaodefroy V, Sobotka V (2021) Coalescence in fused filament fabrication process: thermo-dependent characterization of high-performance polymer properties. *Polym Testing* 98(107096):107096. <https://doi.org/10.1016/j.polymertesting.2021.107096>
 124. Vyavahare S, Kumar S, Panghal D (2020) Experimental study of surface roughness, dimensional accuracy and time of fabrication of parts produced by fused deposition modelling. *Rapid Prototyp* 26(9):1535–1554. <https://doi.org/10.1108/RPJ-12-2019-0315>
 125. Prasong W, Ishigami A, Thumsorn S, Kurose T, Ito H (2021) Improvement of interlayer adhesion and heat resistance of biodegradable ternary blend composite 3D printing. *Polymers* 13(5):740. <https://doi.org/10.3390/polym13050740>